11 Advances in Patch Antenna Design Using EBG Structures

Ekta Thakur, Dr. Naveen Jaglan,
Prof. Samir Dev Gupta
Jaypee University of Information Technology, Solan

Prof. Binod Kumar Kanaujia
Jawaharlal Nehru University, New Delhi

CONTENTS

11.1 INTRODUCTION

High-performance applications in wireless communication systems require an advanced form of electromagnetic materials. The development of "metamaterials" with unique features has recently gained great attention from the researchers [1]. Metamaterials are used in many fields such as optics, nanoscience, material science,

and antenna engineering. These materials have special characteristics that do not exist in naturally occurring materials. Hence, designing metamaterials with unique characteristics and using them in several antenna applications is an interesting concept for researchers. The concept of photonic crystals was introduced by Yablonovitch in solid-state physics [2]. The photonic crystals with a forbidden band gap are used in optics and solid-state physics. Therefore, the term photonic band gap (PBG) of the optics is used as electromagnetic band gap in the microwave domain. EBG structures are classified as a special type of metamaterial and can be defined as periodic or non-periodic structures that prevent or help the transmission of electromagnetic waves in a specific band of frequency [3,4]. EBG structures have many names in the literature, including left-handed materials, soft and hard surfaces, double-negative materials, negative refractive index materials, high-impedance surfaces (HIS), magnetomaterials, and artificial magnetic conductors (AMC) [5]. They are categorized into three groups: (i) three-dimensional volumetric structures, for example woodpile structure, (ii) two-dimensional planar structures, for example mushroom-like EBG structure, and (iii) one-dimensional transmission lines, such as holes in the ground plane. The EBG unit cell has a single band gap; however, a periodic arrangement of EBG structures can have multiple band gaps. In addition to the band gap feature, EBG structures also have some other important characteristics such as AMC and HIS [6]. For example, for both TE and TM polarizations, the two-dimensional EBG structures show a high-impedance surface. And when a wave strikes the EBG surface, 0° reflection phase is obtained and the EBG surface behaves as an AMC. These special features of EBG structures lead to a broad range of applications in microwave and antenna engineering [7,8].

In this chapter, we discuss the recent advancements in patch antenna design using EBG structures. These structures help improve the gain and bandwidth of the patch antennas. They are also used to reduce mutual coupling and to obtain band-rejection characteristics in ultra-wideband (UWB) antennas. A number of techniques to improve the gain and bandwidth, to achieve multi-band characteristics, to reduce mutual coupling, and to obtain multiple band-notch characteristics using compact EBG structures are also discussed later in this chapter. Finally, some real-life applications of EBG structure-integrated patch antennas, such as RFID and wearable electronics, are summarized.

11.2 EBG STRUCTURES AND THEIR PROPERTIES

An EBG structure is made up of metallic patches, ground plane, dielectric materials, and vias that connect patches to the ground plane [6]. From inductance and capacitance, the notch resonance frequency of an EBG cell can be determined using eq. (11.1):

$$f_s = \frac{1}{2\pi\sqrt{LC}} \tag{11.1}$$

where f_s represents the operating frequency of the EBG structure. This operating frequency can be varied by varying the inductance and capacitance. The values of inductor L and capacitor C are evaluated using the given formula [6–8]

$$L = \mu_0 h \tag{11.2}$$

$$C = \frac{W\varepsilon_0(1+\varepsilon_0)}{\pi}\cosh\frac{(2W+g)}{g} \tag{11.3}$$

where W, g, h, μ_0, and ε_0 are the width of the patch, the gap between two EBG structures, the substrate height, the permeability and permittivity of free space, respectively. The EBG structures' band gap can be evaluated by three methods, i.e., reflection phase, dispersion diagram, and the transmission characteristics calculated by suspended line method. Reflection phase characteristics of an EBG unit cell are used to predict the electromagnetic nature of the surface. For perfect electric conductor (PEC) and perfect magnetic conductor (PMC) ground planes, the reflection phase is 180° and 0°, respectively [9]. However, the PMC does not occur in the environment. For an EBG ground plane, the reflection phase varies from +180° to −180° with increasing frequency. The frequency range between +90° and −90° generally overlaps the band gap of an EBG structure [10]. Figure 11.1a indicates the reflection phase. The dispersion diagram, which is calculated using Eigenmode solver, is used to obtain the band gap of periodic EBG structures. The plot of phase constant and resonant frequency is referred to as the dispersion diagram [11]. Figure 11.1b illustrates the dispersion diagram. In the transmission characteristics method, the band gap is calculated by replacing the PEC ground plane with the EBG array. Figure 11.1c indicates the transmission loss. Transmission losses less than −15 dB are generally considered as the band gap of the EBG structure [12]. The transmission characteristics and reflection phase are enough for calculating the band gap of an EBG structure. From the transmission characteristics and reflection phase, the AMC at 0° and the surface wave band gap of the EBG structure can be easily recognized [13]. The dispersion diagram consumes more memory and time, but gives more information on band gap.

11.3 EBG STRUCTURES IN PATCH ANTENNA DESIGN

For wireless communication application, patch antenna are mostly preferred due to its low profile and low cost with high performance. The patch antennas have major benefits such as ease of installation, low cost, low profile, and integration with printed circuits. Some of the drawbacks of patch antennas are low efficiency, low power, high Q, surface wave excitation, and narrow bandwidth [15]. The unique features of the EBG structure are found useful to overcome the drawbacks of a patch antenna. The EBG structure helps in gain and bandwidth improvement [16–19]. In general, an EBG patch antenna produces a plane radiation profile, fewer side lobes, and a good antenna efficiency compared to a normal patch antenna. The EBG structure also ensures low interference to the adjacent elements and acts as a shielding material between the antenna and the communication system user. Further, the EBG structure has also been used in MIMO [20–22] systems and array antennas to alleviate the mutual coupling [23] effect. The application of EBG structures in patch antennas is a smart research area; however, some problems arise as two different structures are combined together to achieve enhanced performance. Some

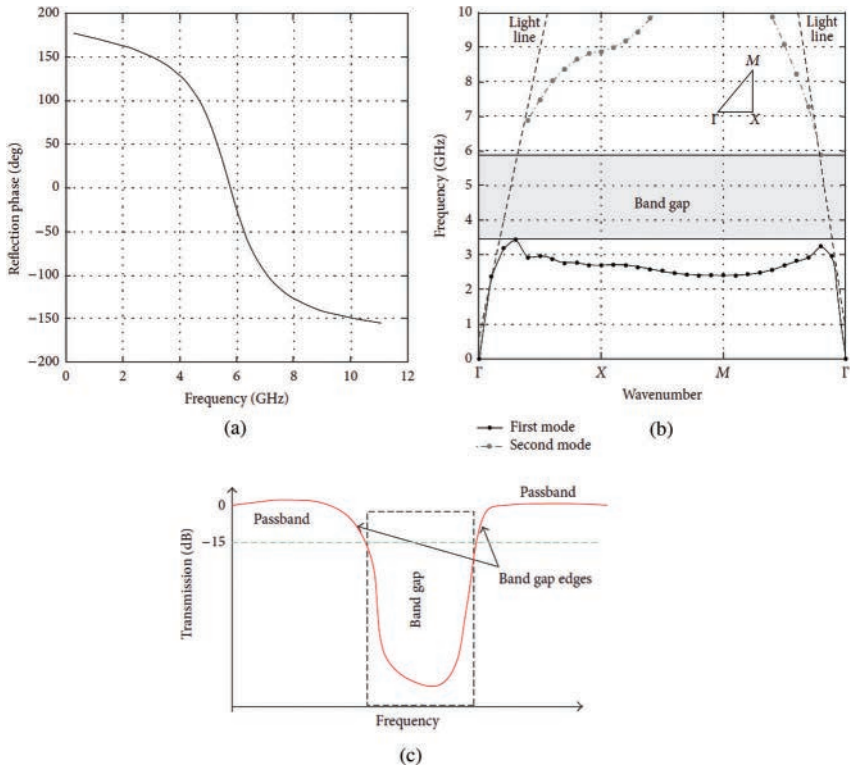

FIGURE 11.1 Different methods for calculating the band gap: (a) reflection phase methods (b), dispersion diagram methods, and (c) transmission characteristics methods [14].

new designs and their applications to enhance the performance of patch antennas are discussed in this chapter.

11.3.1 Bandwidth Improvement in Patch Antennas Using EBG Structures

For wireless communication systems, the mostly preferred antenna is the patch antenna. Generally, the conventional patch antenna has narrow bandwidth because of the PEC material in the ground plane. To achieve a wide bandwidth, the researchers have done intensive research and suggested a number of EBG structures. A wide band of 3–35 GHz is achieved by placing a periodic structure of circular and square EBG patch around the half-circular monopole antenna [24]. By inserting the conventional mushroom-type EBG structures on either side of the feed line, the impedance bandwidth is increased by 0.1 GHz as compared to the monopole UWB antenna. A good improvement in bandwidth is obtained by etching dummy EBG patterns on the feed line [25] as shown in Figure 11.2.

The EBG array is inserted on a substrate with a height of 0.4 mm and a dielectric constant of 2.33. The patch size is 8 mm × 6.3 mm, resulting in an operating frequency

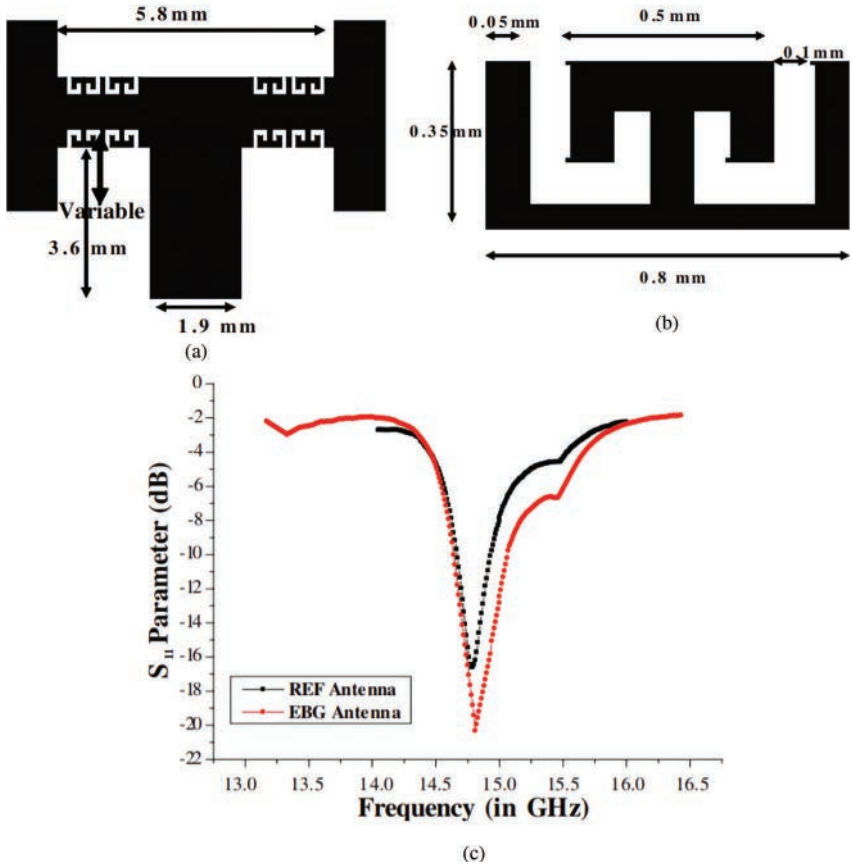

FIGURE 11.2 (a) Magnified view of feed line and (b) magnified view of EBG pattern [25] (c) S11 parameters Vs frequency.

of 14.8 GHz. Eight rows of dummy EBG structures are etched on the patch feed line with a gap of 5.8 mm in between two patches. The test data show the improvement in the bandwidth of over 0.381 GHz. In [26], Fabry–Perot (FP) antennas were integrated with EBG metamaterials for getting 4.92% impedance bandwidth and 10.7 dB gain simultaneously [27]. From Figure 11.3, it can be seen that using a trapezoidal ground plane in combination with a uniplanar EBG structure [28] increases the bandwidth and also improves the radiation characteristics of a monopole antenna. By changing the width of an EBG structure, one can vary its operating frequency. The total volume of the antenna is $100 \times 75 \times 0.762$ mm^3 including eight EBG cells. A conventional mushroom-type EBG structure was modified by inserting multiple vias to increase the band gap for noise suppression [29,30]. As shown in Figure 11.4, four vias are optimized to achieve a wider band gap and it is termed as ground surface perturbation lattice (GSPL) [31]. Figure 11.5 illustrates a lotus flower patch attached to a wide transmission line with an EBG ground plane to increase the bandwidth of the antenna. A slanted ground plane with an EBG structure was used to enhance the

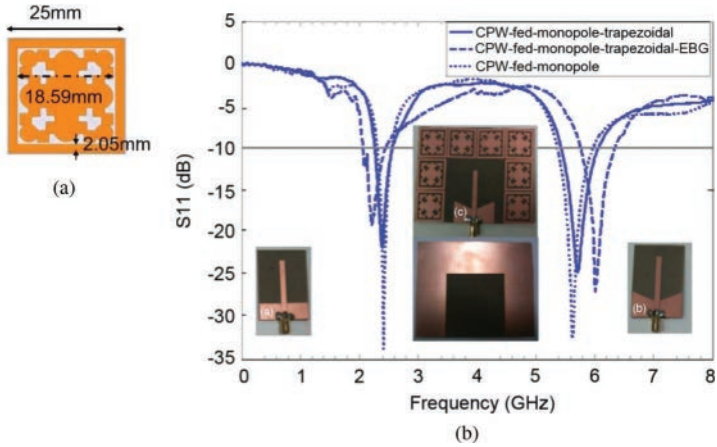

FIGURE 11.3 (a) Dual-band EBG structure; (b) return loss measurements [27].

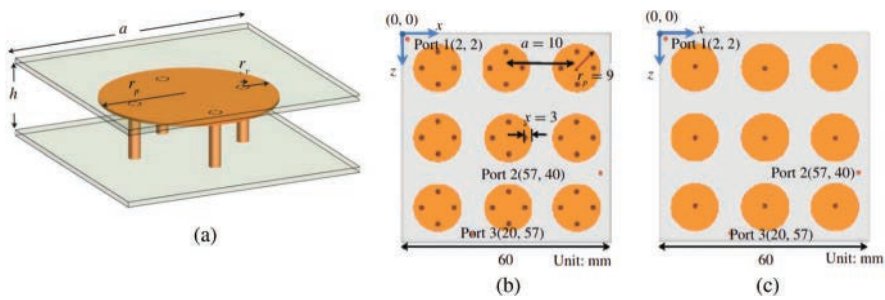

FIGURE 11.4 (a) Side view of GSPL structure; (b) GSPL structure. (c) Two-dimensional EBG structure [31].

bandwidth of the elliptical and rectangular monopole antennas [32]. In the literature, to enhance the bandwidth, a multilayer EBG structure [33] was also used. Monopole antennas of different shapes such as elliptical [34] and semi-circular [35] were suggested for enhancing the bandwidth. Further, the bandwidth of an UWB antenna can be improved by using EBG structures with a monopole antenna. Thus, in Table 11.1, some of the EBG structure approaches are described for bandwidth improvement.

11.3.2 Gain Improvement Using EBG Structures

With the arrival of new wireless communication services, the demand for ultra-wideband with low cost and compact size is increasing tremendously. The main drawbacks of printed antennas are low gain and low radiation efficiency because of the propagation of the surface wave. If an antenna is placed over a PEC ground plane such as copper or gold, it starts radiating into space. Additionally, it also produces currents that move along the sheet. These currents are also called surface waves and propagate to an edge of the antenna surface and cause multi-path interference.

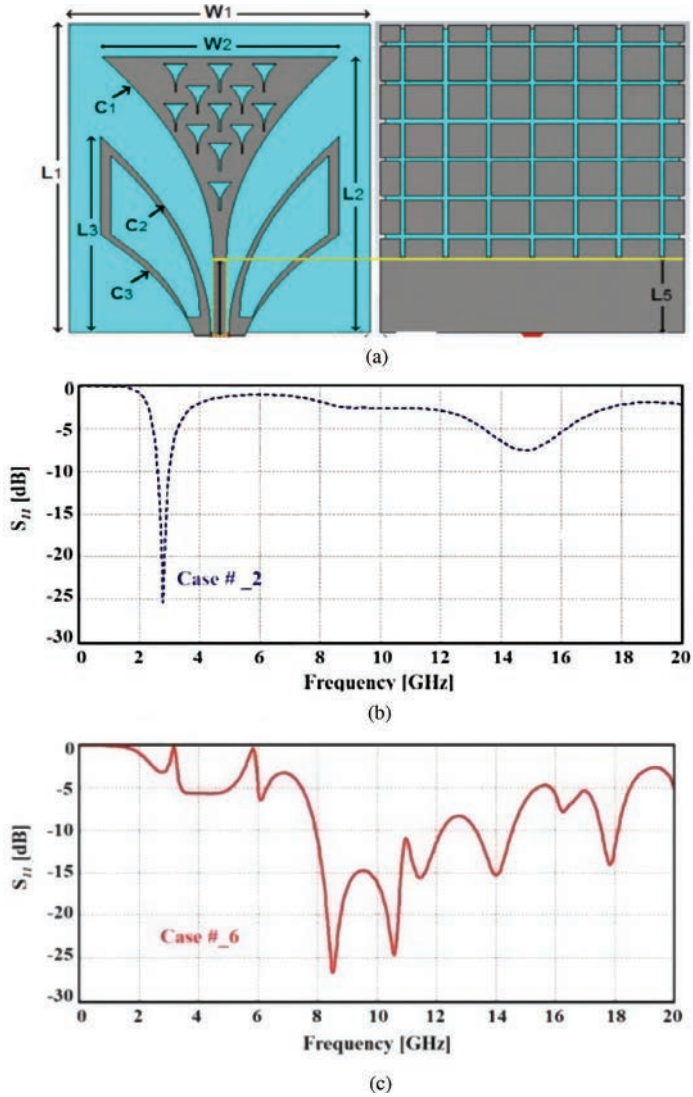

FIGURE 11.5 (a) Lotus-shaped antenna with an EBG ground plane, (b) $|S_{11}|$ of lotus-shaped antenna with partial ground plane, (c) $|S_{11}|$ of lotus-shaped antenna with EBG ground plane [32].

A number of approaches to increase the gain of patch antennas using EBG structures have been proposed. In these approaches, the EBG structure is designed in a way that its band gap and antenna resonant frequency band overlap. As a result, the surface waves cannot propagate along the substrate and the amount of radiating power increases. In order to improve gain, the EBG structure can be placed in two ways – the first is by placing the EBG structure around the patch antenna, which is [36] termed simply as the EBG structure, and the second is by replacing the ground plane with the EBG structure which is called AMC [37]. A double-rhomboid bow

TABLE 11.1
Bandwidth Enhancement Using Different EBG Approaches

S. No.	EBG Approach	Reason	Reference
1.	EBG pattern on the feed line	Bandwidth is improved due to impedance matching	[25]
2.	Multilayer EBG structure	Merging multiple bands into one wide band gap	[30,36]
3.	Symmetric placement of EBG structure around the patch	Bandwidth enhancement due to the different resonant frequencies	[28]
4.	Multiple-via EBG structure	By increasing inductance, reflection phase behavior gives much wider bandwidth	[32]
5.	EBG ground plane	To couple between the patch and EBG-AMC resonance frequencies	[24,27,33,34]

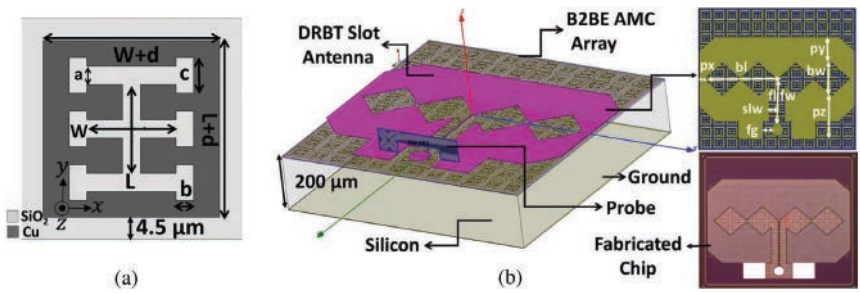

FIGURE 11.6 (a) EBG structure; (b) antenna with AMC array [38].

tie-slot antenna [38] was presented with an end-to-end E-shaped EBG surface for gain improvement at the W-band, as shown in Figure 11.6. This EBG surface behaves as a reflective surface that helps to improve the gain of the on-chip antenna. To prevent the losses due to waves entering into the lossy silicon substrate, an AMC array surface is placed beneath the patch. In another interesting study, a low-temperature co-fired ceramic (LTCC) patch antenna's gain was improved using a Sievenpiper EBG structure [39]. This LTCC was designed to resonate at 60 GHz on a DuPont™ Greentape™ 9K7 ($\varepsilon_r \sim 7.0$) of 5 mm thickness.

The two-element LTCC patch array was combined together with the Sievenpiper EBG structure to eliminate surface waves. As a result, around 4 dBi of gain enhancement and 8 dB of reduction in side lobe level were obtained, as shown in Figure 11.7. The design of eight-element MIMO antennas for 5G applications such as smartwatch and dongle [35] is presented in Figure 11.8. To improve gain and efficiency, an EBG surface was used as a ground plane. The upper layer of the substrate has eight MIMO antennas [36–40], whereas the bottom layer is composed of an EBG ground plane. The gain and antenna efficiency obtained were 8.732 dB and 92.7% at the resonant frequency, respectively.

Another study was performed [40] by changing the vias' positions in different patterns in the EBG ground surface, as presented in Figure 11.9a–d, and it was found

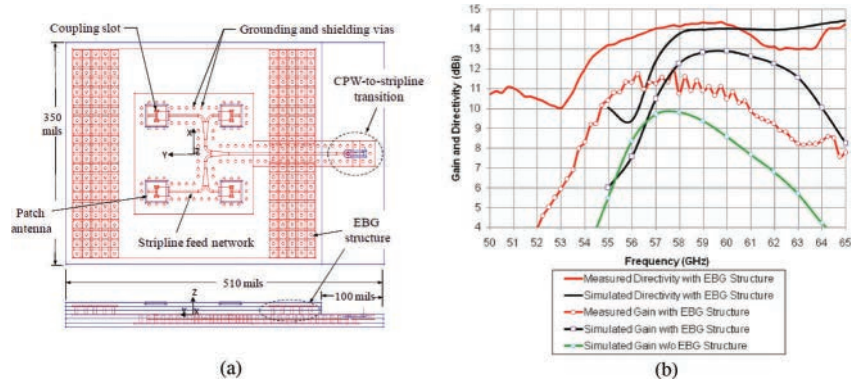

FIGURE 11.7 (a) 2×2 patch array; (b) gain and directivity versus frequency of the 2×2 patch array [39].

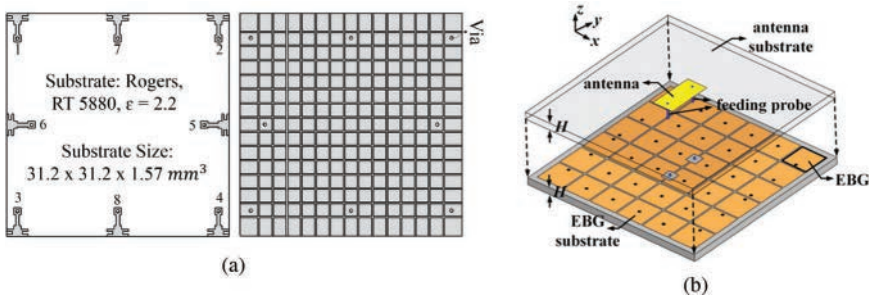

FIGURE 11.8 (a) Top and bottom views of an eight-element MIMO antenna with EBG ground plane [35]; (b) 3D view of cylindrically projected EBG planes [40].

that the antenna gain and efficiency were improved by 14.1 dB and 107.2%, respectively. Besides improving gain and directivity, the EBG superstrate also obtains dual-band dual-polarization [41–43] and suppresses the grating lobes in array antennas. Different EBG structures [42–48] were discussed based on the position of the EBG structure, such as below the patch and around the patch, to improve the overall performance of the antenna. In [49], a slotted EBG structure was used to improve the gain and to reduce the radar cross section (RCS) of a patch antenna. This slotted EBG structure was made of arrays of mushroom-type structure with rectangular slots on the patch. From the tested results, it was observed that the gain improved by 2.5 dB and RCS reduced to 4.3 dB as compared to the conventional patch antenna. Thus, few EBG structure approaches are discussed in Table 11.2 to improve patch antenna gain.

11.3.3 Mutual Coupling Reduction Using EBG Structures

Mutual coupling between antenna elements is due to the propagation of surface waves, and it affects the overall performance of the antenna. In case of a patch antenna, the E-plane coupling is stronger than the H-plane coupling. Several

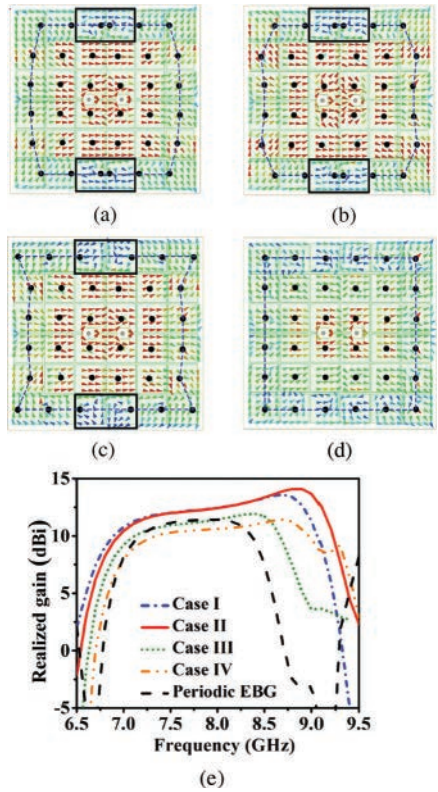

FIGURE 11.9 (a–d) Different patterns of vias in EBG ground plane; (e) realized gain of different EBG planes [40].

TABLE 11.2
Gain Enhancement Using Different EBG Structure Approaches

S. No.	EBG Structure Approach	Reason	Reference
1.	EBG structure placed around the patch	Surface wave suppression results in improved gain	[38,42,44,47,48]
2.	EBG structure ground plane	AMC property is utilized as a reflector	[35,40,49]
3.	Superstrate EBG structure layer above the patch antenna	Multiple reflections in cavity result in performance enhancement	[50,51]

methods were discussed and applied to reduce the mutual coupling between the MIMO system and antenna array, which include defected ground plane, decoupling strips, and neutralization line. For the MIMO system, it is desirable to have a mutual coupling of less than 15 dB, the envelope correlation coefficient (ECC) should be less than 0.5, and the total active reflection coefficient (TARC) should be less than 0 dB. The ECC is used to measure the correlation between radiation patterns of

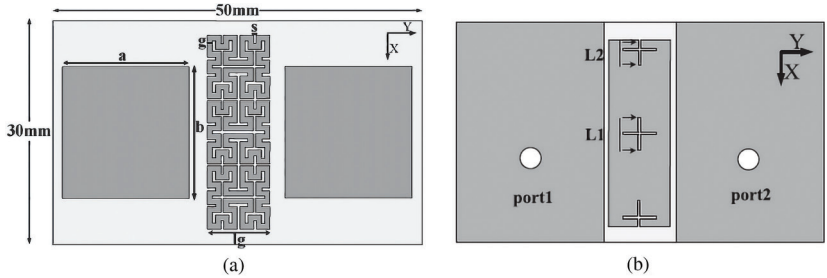

FIGURE 11.10 (a) Top view and (b) back view of patch antenna array [52].

MIMO antennas. The TARC is similar to return loss, but also considers the effect of mutual coupling. In [52], the mutual coupling was reduced by using two fractal uniplanar compact EBG structures and three cross-slots in between the patch arrays, as shown in Figure 11.10. By placing the two rows of fractal uniplanar compact EBG structure on the top layer, the mutual coupling was reduced 13 dB. Moreover, etching three cross-slots on the ground plane further improves the reduction in the mutual coupling. In [53], the conventional uniplanar compact EBG structure was modified by inserting rectangular slots. The modified EBG is shown in Figure 11.11a. Two-element MIMO antennas [53] were designed in a way that one element is positioned in front of the other. The introduction of the modified EBG array amid the two patches eliminated the propagation of surface waves. A parallel connection of L and C with series L and C connections formed a narrow band-stop filter. Because of the parallel inductance connections, the overall inductance decreased, and due to the parallel capacitance connections, the overall capacitance increased. These parallel connections aided in reducing the isolation by increasing the quality factor. The relation, given in eq. (11.4),

$$Q = \eta\sqrt{\frac{C}{L}} \tag{11.4}$$

Another investigation accomplished in [54] considered the planar compact EBG structure. To achieve better mutual coupling reduction, the planar EBG structure is placed in three different arrangements as shown in Figure.11.12. The planar compact EBG structure was fabricated using an FR4 substrate with a height of 1.6 mm and an overall dimension of 5.05×6.52 mm^2. The operating frequency of the antenna was nearly 5.6 GHz, which is at the WLAN band. In [56], a split EBG structure was placed amid the patch elements and the mutual coupling was decreased by 28 and 45 dB at 3.49 and 4.788 GHz, respectively. The split EBG structure is illustrated in Figure 11.13. In [55], miniaturized two-layer EBG structures were studied for decreasing the mutual coupling between UWB monopoles. These EBG structures contained slits in the ground plane, and as the number of slits increased, the electromagnetic coupling reduced. Figure 11.14 shows the variation in the mutual coupling with the number of slits in the ground plane. Table 11.3 shows the different EBG structures discussed in the literature to reduce the mutual coupling..

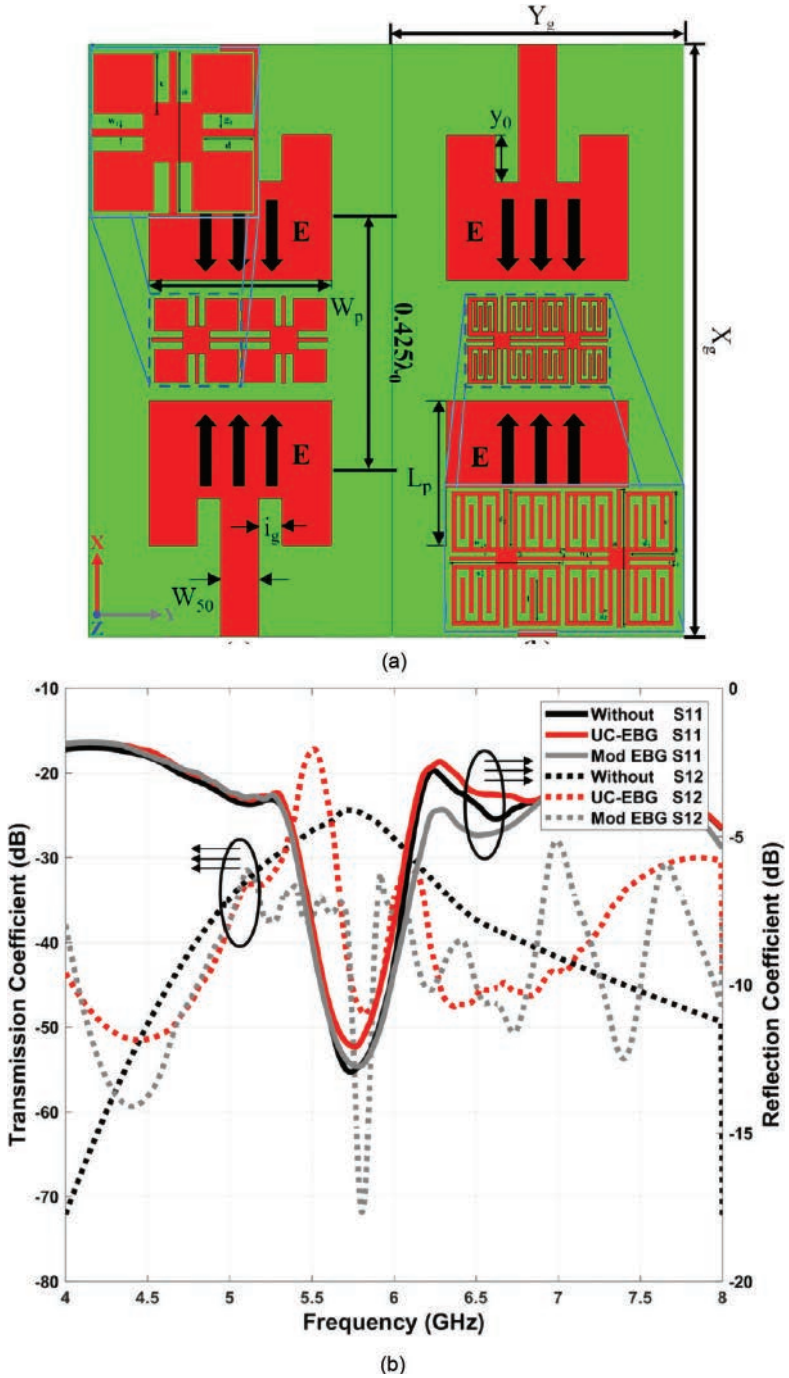

FIGURE 11.11 Two-element UWB MIMO antenna with inset feed: (a) UC-EBG structure and the proposed modified EBG structure; (b) *S*-parameters of three different cases [53].

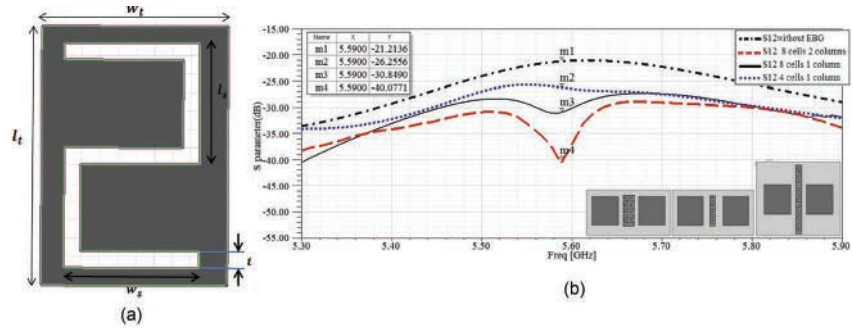

FIGURE 11.12 (a) Planar compact EBG structure; (b) mutual coupling of EBG structure array in three different arrangements [54].

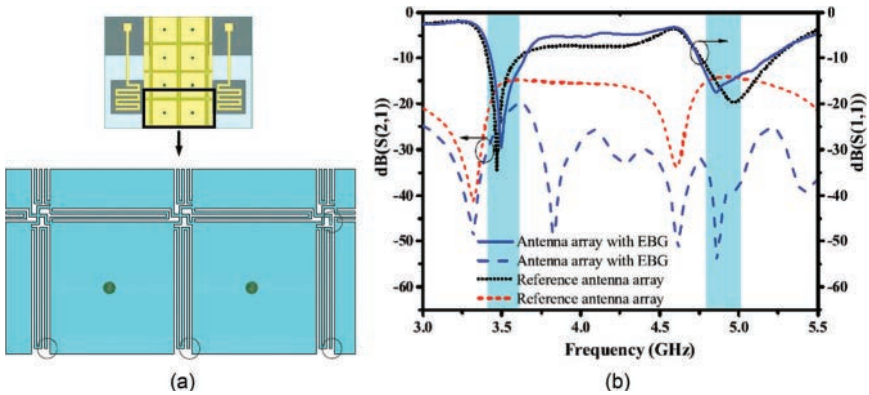

FIGURE 11.13 (a) Two-element meander line antenna; (b) reflection coefficient and mutual coupling with and without split EBG structure [56].

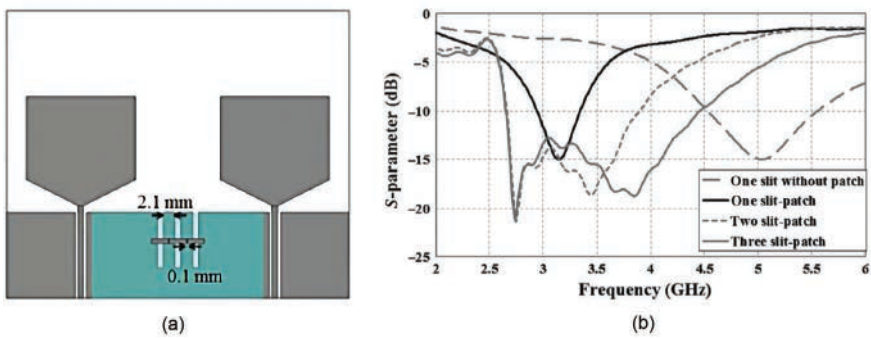

FIGURE 11.14 (a) Planar monopole MIMO antenna; (b) variation of mutual coupling [55].

TABLE 11.3
Mutual Coupling Reduction by Using Different EBG Structures

S No.	Type of EBG Structure	Mutual Coupling	Dielectric Constant (ε_r)	Height (mm)	Reference
1.	Fractal uniplanar compact EBG structure	−37 dB	2.65	1	[52]
2.	Modified EBG structure	−70 dB	4.4	1.6	[53]
3.	Planar compact EBG structure	−28 dB	4.8	1.6	[54]
4.	Double-layer EBG structure	−22 dB	4.5	1.55	[55]
5.	Split EBG structure	−44 dB	4.4	1.2	[56]
6.	Uniplanar compact EBG structure	−28 dB	10.2	1.27	[59]
7.	EM band gap metamaterial	−37 dB	4.3	1.6	[60]
8.	Uniconductor EBG structure	−46 dB	4.4	1.6	[61]
9.	Tunable double-layer EBG structure	−45 dB	4.5	1.55	[62]

11.3.4 Band-Notch Operation in Patch Antennas Using EBG Structures

In April 2002, FCC unbound the frequency range that lies from 3.1 to 10.6 GHz and this band is termed as UWB. Some narrowband communication systems (WiMAX, WLAN, and X-band) also work within this range, which produces interference. Many different design methods have been presented in the literature to avoid interference. The methods such as etching slots and using stubs and resonators, such as capacitively loaded loop and electric ring, disturb the radiation pattern because of discontinuities in the radiating elements. This problem can be solved by using the band-rejection characteristics of EBG structures. By inserting the EBG structure near the feed line of the UWB antenna, the interference of narrowband communication can be discarded [57]. In the literature [58], various designs of EBG structures have been presented to obtain band-notch characteristics. A swastika-type EBG structure [63] was used to achieve single-band-notch characteristics with a band gap of 7.5–11.1 GHz. In [64], by placing the EBG structures near feed line, three notches at WiMAX (3.5 GHz) and WLAN (5.2/5.8 GHz) bands are achieved. Mushroom-type EBG structures with vias at center [65] and edge-located mushroom-type EBG structures [65–68] are some structures presented by the researchers. A uniplanar EBG structure and two mushroom-type EBG structures [70] were placed near the feed line of the monopole antenna to have triple-band-rejection characteristics. A hexagonal-shaped c-slot mushroom-type EBG structure [66] was used to achieve band-notch function for X-band satellite communication systems (6.7–7.7 GHz). In [71], four EBG structures were placed close to the feed line to attain dual-band-notch characteristics [72], as shown in Figure 11.15a. The patch antenna and EBG structure were fabricated on a cheap FR4 substrate of dimensions $58 \times 45 \times 1.6$ mm^3. Figure 11.15b indicates the VSWR of an UWB MIMO antenna. In another interesting study [74], a circular monopole antenna [75–77] with two mushroom-type EBG structures was used to obtain band-notch characteristics for WLAN and WiMAX. Moreover, 34% of compactness was also achieved by etching an L-shaped slot on the EBG surface.

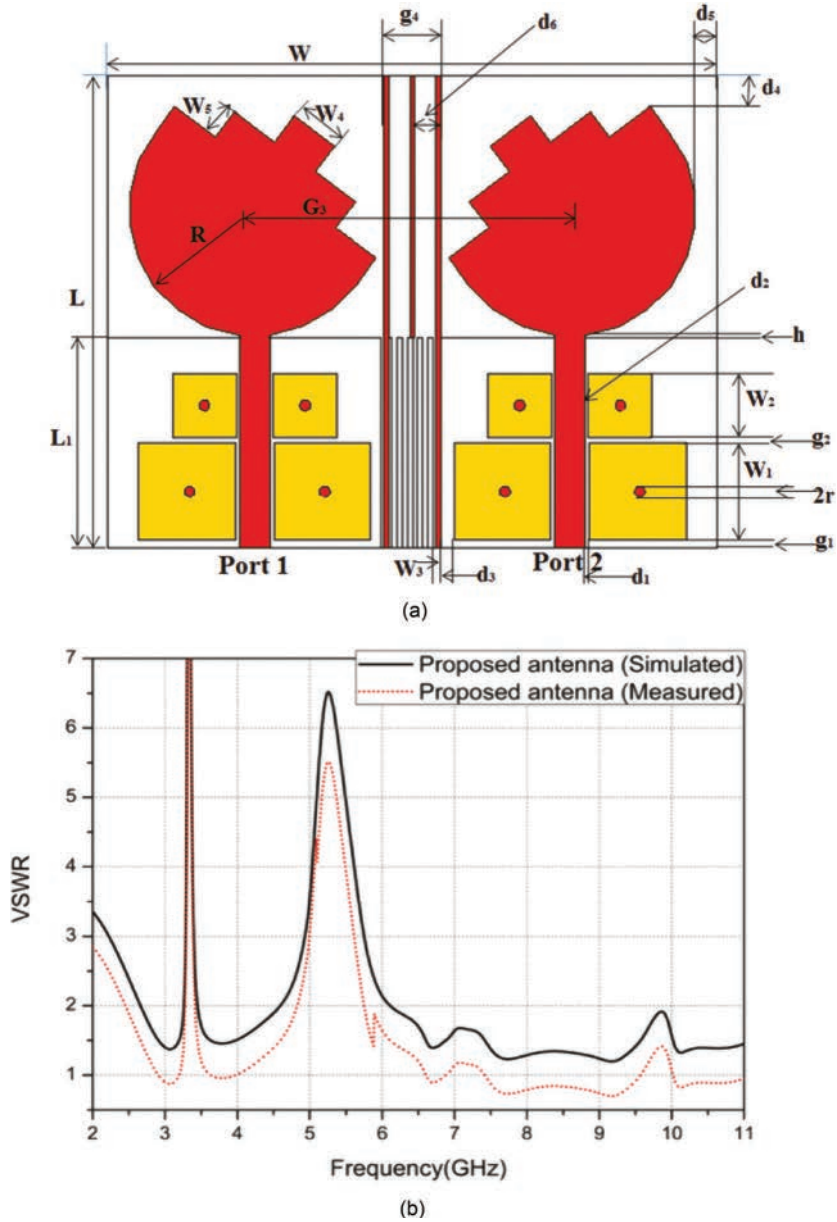

FIGURE 11.15 (a) Band-notched UWB MIMO antenna; (b) VSWR plot [71].

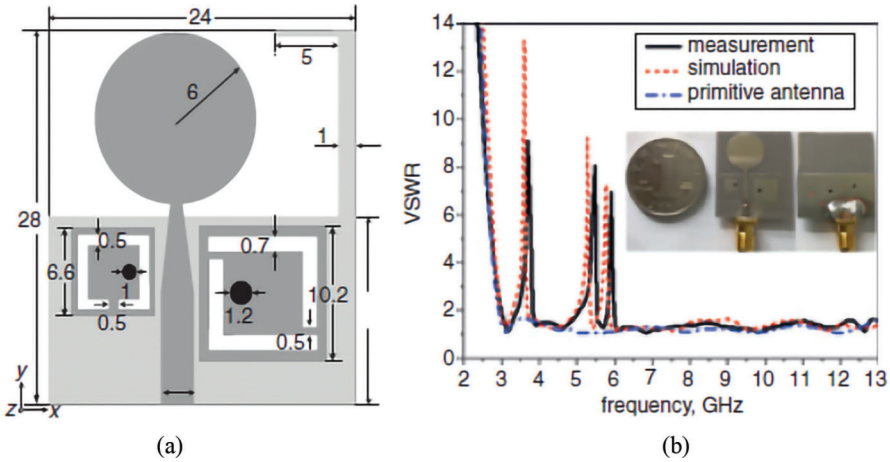

FIGURE 11.16 (a) Triple-band-notched monopole UWB antenna; (b) VSWR plot [74].

Figure 11.16a shows a circular monopole antenna with two modified EBG structures. This modified EBG structure contains two L-shaped slots with an edge-located via (ELV) that achieve two notched bands. So, in this, a single EBG structure is used to obtain dual-band-notch characteristics. A dual-band-notched MIMO antenna obtains notches in WiMAX band (3.3–3.6 GHz) and WLAN band (5–6 GHz), as presented in Figure 11.16b. A triple-band-notched UWB MIMO antenna [70] was realized by using three EBG structures. Figure 11.17 indicates the band-notched antenna. The designed antenna avoids the interference from WiMAX band ranging from 3.3 to 3.6 GHz, WLAN band ranging from 5 to 6 GHz, and the X-band for satellite communication systems ranging from 7.2 to 8.4 GHz. Another modified EBG structure connected with the feed line was used to reject the interference from narrowband communication systems [73]. This modified EBG structure also rejects are for WiMAX, WLAN, and X-band satellite communication system.

This single EBG structure rejects are for WiMAX, WLAN, and X-band satellite communication systems. Figure 11.18a displays the band-notched UWB antenna. The antenna and EBG structure are designed using a FR4 substrate with a height of 1 mm, a dielectric constant of 4.4, and an overall dimension of $30.5 \times 26 \times 1$ mm^3 and 8×5.95 mm^2, respectively. A pentagonal printed UWB monopole antenna having three notched bands is shown in Figure 11.19a. Two slots are inserted in the EBG structure to attain multiple band rejection. The dimension of the EBG structure is 9.4×4.5 mm^2. Figure 11.19b indicates the VSWR of the band-notched UWB antenna. Thus, Table 11.4 shows several cases of different EBG structures for achieving band-notch characteristics.

11.3.5 Dual-Band and Multi-Band Characteristics Using EBG Structures

In the previous section, numerous EBG structures were discussed to improve bandwidth and gain, to reduce mutual coupling, and to obtain band-notch characteristics.

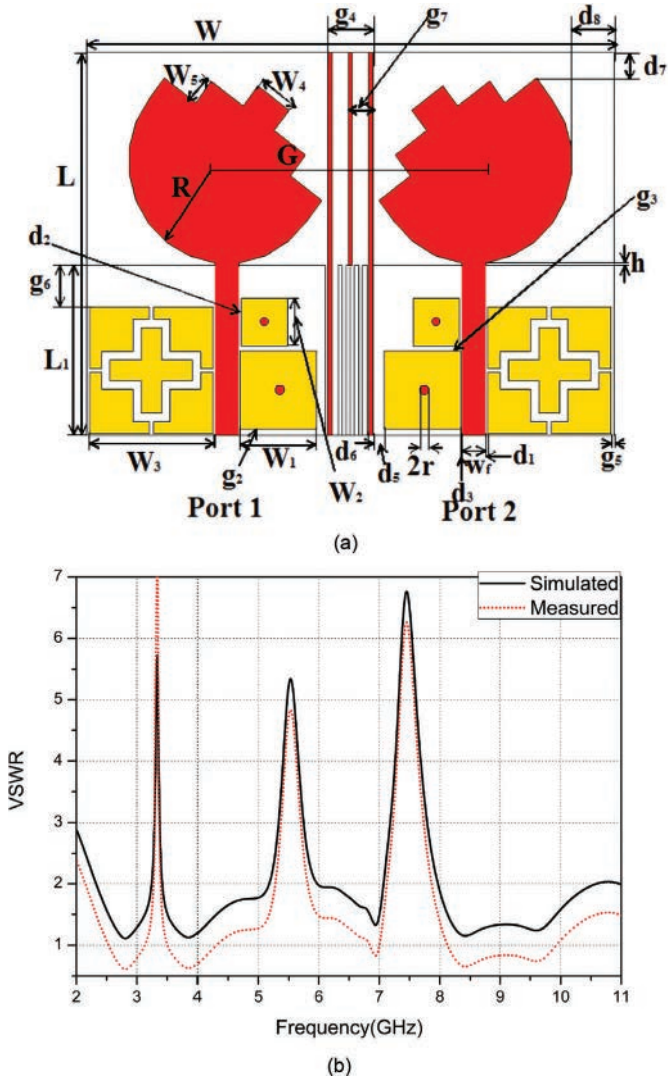

FIGURE 11.17 (a) Triple-band-notched UWB MIMO antenna; (b) VSWR plot [70].

The motivation of this section is to study the idea of multi-band operation in patch antennas using EBG structures. The resonant frequency of EBG structures can be calculated using a distributed lumped network. Using this distributed lumped network, the researchers have designed numerous EBG structures to obtain dual-band and multi-band characteristics in patch antennas.

In [79], dual-band characteristics were obtained by placing pinwheel-shaped slot EBG structure periodically around the antenna. The antenna combined with periodical EBG structures resonated at 4.9 and 5.4 GHz. The tested result also showed a bandwidth improvement of 41% and 25.4% at low frequency and high frequency,

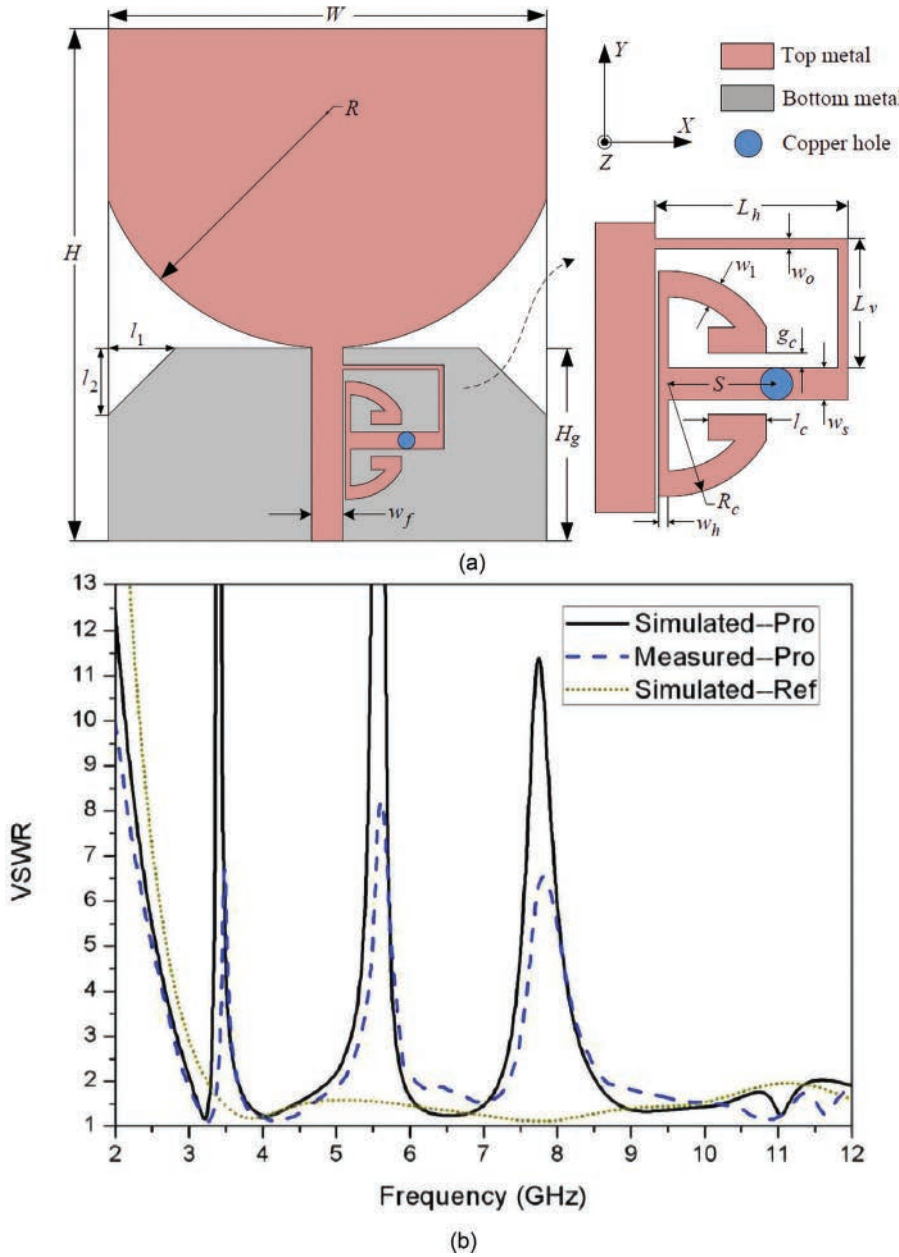

FIGURE 11.18 (a) Band-notched UWB antenna; (b) VSWR of triple-band-notched UWB MIMO antenna [73].

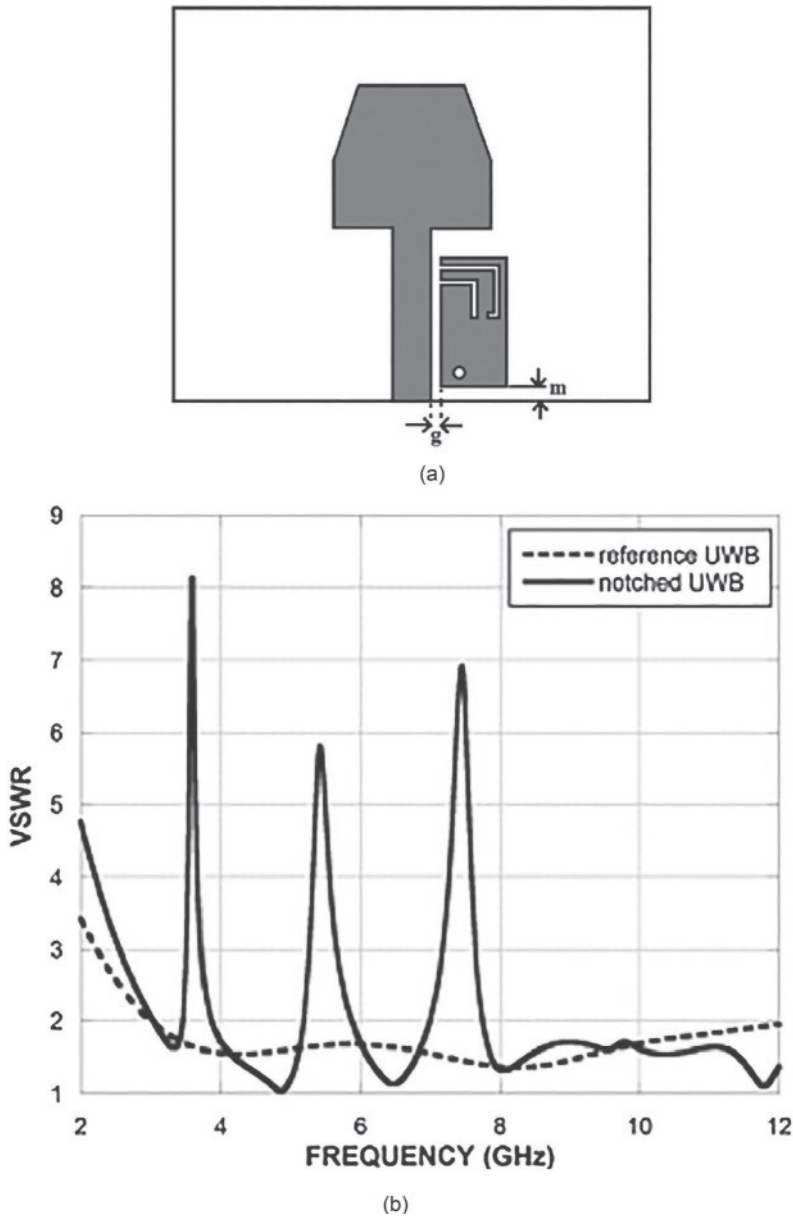

FIGURE 11.19 (a) Pentagonal UWB monopole antenna; (b) VSWR plot [75].

TABLE 11.4
Band-Notch Characteristics by Using Different EBG Structures

S. No.	No. of Notches	Type of EBG Structure	Notched Band (GHz)	Size (mm²)	Reference
1.	Single-notched band	Mushroom EBG structures	5.36–6.34	6.25×6.25	[22]
2.	Triple-notched band	Mushroom EBG structures and two split ring resonators	6.7–7.7	3.9×3.9	[66]
3.	Dual-notched band	Mushroom EBG structures	3.3–3.6 5–6	9.25×9.25 6.1×6.1	[76]
4.	Dual-notched band	DG-CEBG	3.3–3.6 5–6	5×5 3×3	[77]
5.	Dual-notched band	Uniplanar EBG structures with a π-shaped slot	3.45–3.9	5.2×5.2	[78]
6.	Triple-notched band	Uniplanar EBG structure Mushroom EBG structure	3.3–3.6 5–6 7.1–7.9	15×15 9.25×9.25 5.6×5.6	[79]

respectively. Figure 11.20 illustrates the H-shaped MPA with pinwheel-shaped slot EBG structures and the VSWR of three different cases. Another study performed in [80] presented a polarization-dependent EBG structure, as presented in Figure 11.21. This EBG structure behaves as a reflector of a dual-band dipole antenna. This reflector transforms the linearly polarized wave into a circularly polarized wave [80]. The tested antenna attained impedance bandwidths and axial ratio bandwidths of 13.4% and 3.2% and 2.4% and 3.5%, respectively. Another dual-polarized dual-band patch antenna was designed by loading a modified mushroom-type EBG unit cell [81], as presented in Figure 11.22. A square slot was etched from the radiating patch antenna, and the modified mushroom unit cell was placed at the slot to attain triple-band characteristics [82]. A new interesting study was performed in which the PEC ground plane was replaced by an EBG surface to obtain dual-band characteristics. The dual-polarized dual-band patch antenna and its simulated and tested results are presented in Figure 11.23. Thus, Table 11.5 lists several cases of EBG structures for obtaining multi-band/dual-band characteristics of patch antennas.

11.3.6 A Low-Profile MPA Using EBG Structures

In wireless communication systems, the dimension of the patch antenna depends on the resonating frequency. In this condition, it is a challenge to design the smallest possible antenna at low frequency. If the total thickness of the antenna is less than one-tenth of the operating wavelength, then the antenna is called a low-profile antenna.

The mutual coupling effect of the nearby ground plane degrades the overall performance. In [81], the performance of an MPA was examined by placing three different ground planes, namely PEC, PMC, and EBG, with the same height. When PEC

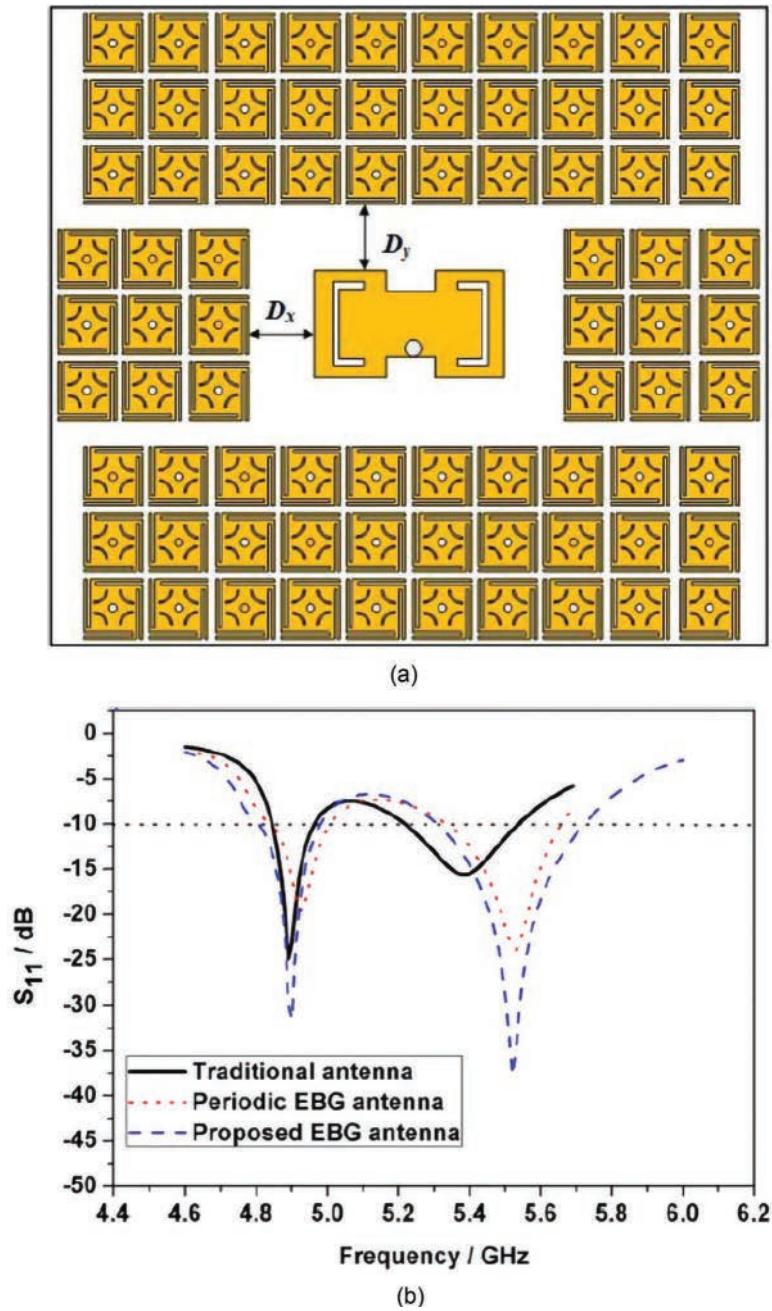

FIGURE 11.20 (a) Patch antenna with coaxial feed; (b) VSWR plot of microstrip antenna [79].

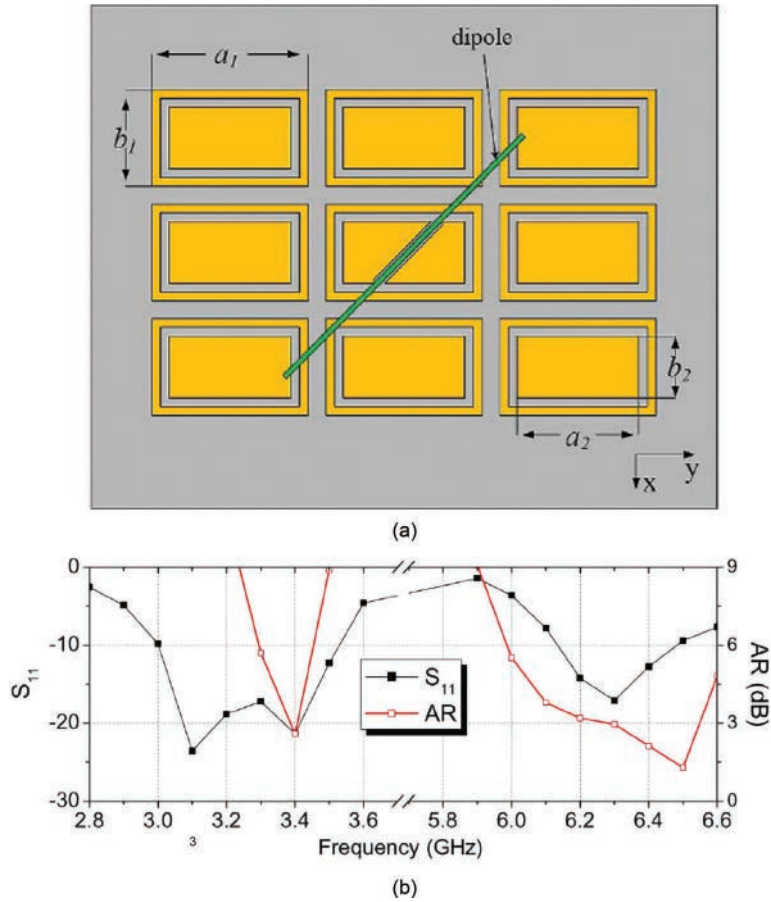

FIGURE 11.21 (a) Circularly polarized antenna; (b) S_{11} parameter and axial ratio plot [80].

TABLE 11.5
Multi-Band/Dual-Band Characteristics by Using Different EBG Structures

S. No.	Type of EBG Structure	Resonating Band without EBG Structure (GHz)	Resonating Band with EBG Structure (GHz)	Reference
1.	Dual-band EBG structure	2.265–2.563 and 5.434–6.061	2.062–2.453 and 5.765–6.343	[33]
2.	Pinwheel-shaped EBG structure	4.85–4.96 and 5.20–5.52	4.82–4.97 and 5.31–5.72	[79]
3.	Modified mushroom-like unit cell	2.21–2.29 and 2.45–2.5	2.21–2.29, 2.34–2.39 and 2.5–2.55	[81]
4.	Spiral conductor EBG structure	2.12–3.35 and 6.01–7.16	2.12–2.98, 5.24–5.80 and 6.05–7.77	[82]
5.	Uniplanar EBG structure	1.7–5.63 and 9.9–11.36	1.5–5.63 and 9.52–13.06	[83]

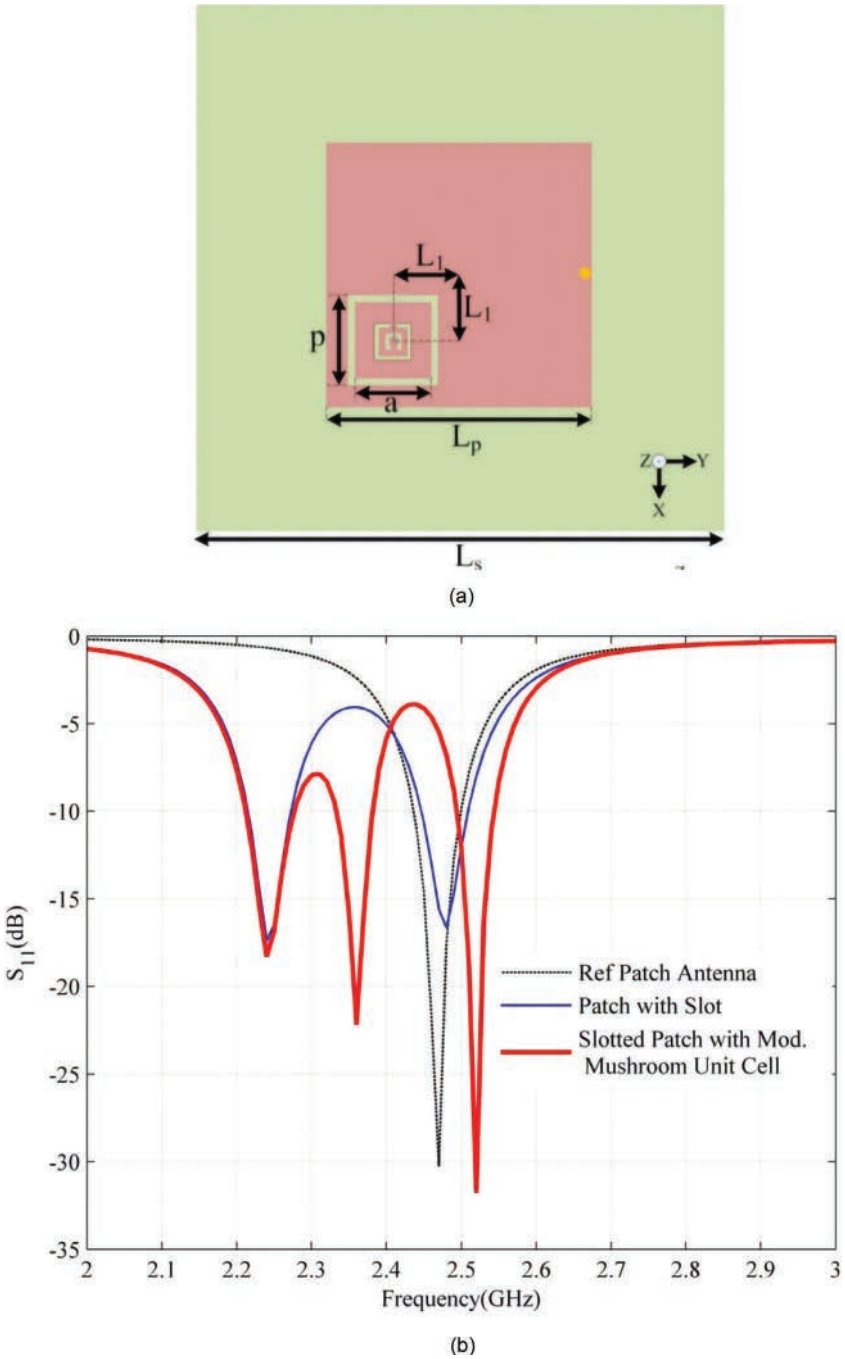

FIGURE 11.22 (a) Dual-polarized dual-band PA; (b) return loss of dual-polarized dual-band PA [81].

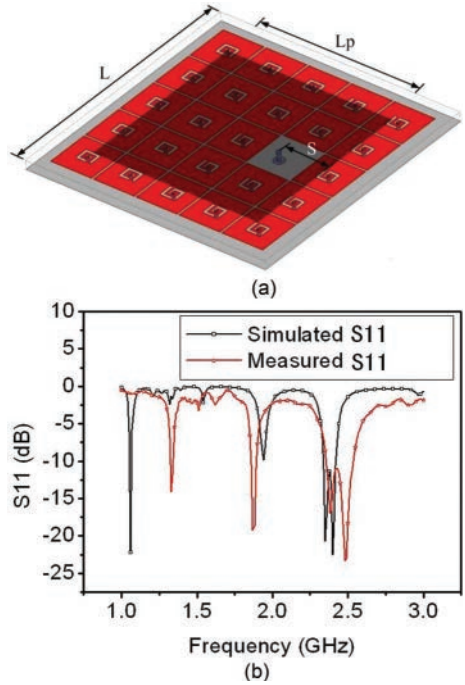

FIGURE 11.23 (a) Multi-band patch antenna; (b) return loss plot [82].

materials such as copper and gold are used as the ground plane, the return loss is −3.7 dB. The reason is that the PEC surface has a reflection phase of 180° and the image current has the opposite direction to that of the printed antenna. The reversal image current cancels the radiation from the printed antenna, resulting in poor return loss. When the ground plane is a PMC, the reflection phase is 0°. But the strong mutual coupling between the patch and image current results in a mismatch between the 50-Ω transmission lines [82]. Only if a proper impedance transformer is used, a good return loss can be obtained. Moreover, the PMC is an ideal surface and does not occur in the environment. However, when the ground plane is replaced by an EBG surface, the reflection phase varies from −180° to +180° and results in constructive interference of image current and radiation from the printed antenna [83–85]. The best return loss of −30 dB is obtained by the printed antenna over the EBG ground plane. From the above discussion, it is observed that the EBG ground plane has the desired features to design low-profile antennas. In [86], a dual-band, low-profile antenna with mushroom-like structures loaded with circular slots was described and is shown in Figure 11.24a. From Figure 24b, we can observe that the first resonating frequency shifts toward the right in case of EBG-CS that leads to compact size at low frequency. By using an EBG-CS superstrate, a low-profile antenna was achieved. In another study, a printed slot antenna placed above an AMC plane was used to obtain a low-profile, wideband antenna [87]. The radiating slots are shown in Figure 11.25a, with three unequal arms that are etched for widening the impedance bandwidth.

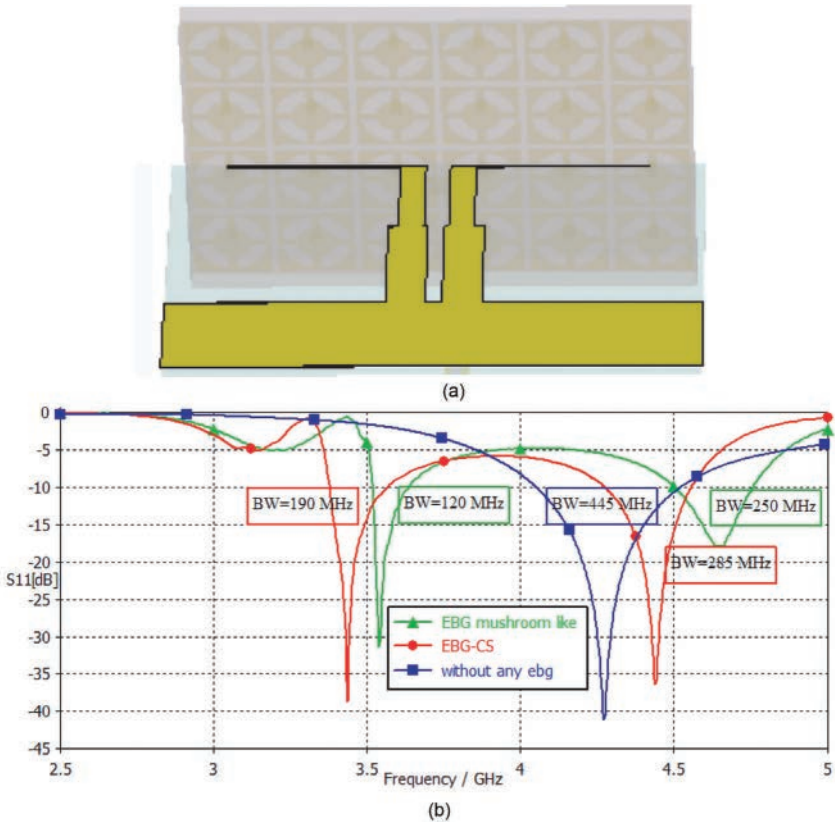

FIGURE 11.24 (a) Dual-band antenna with mushroom-like structures loaded with circular slots; (b) return loss of three different cases [86].

By placing an AMC [88,89] array as the ground plane, the radiation pattern was improved. Using an AMC with a printed antenna resulted in 62.82% compactness in size, a bandwidth improvement of 41%, and a perfect impedance matching. In [90–92] EBG structures that can generate adjustable bandgaps. The EBG structures can be placed as AMC in modern electronic products and potentially cover multiple frequency bands of wireless communications. Similarly, in [93], an AMC array was placed as a ground plane underneath a dual-wideband circularly polarized [80,94] antenna to achieve a low-profile antenna.

Two barbed-shape and bow tie dipoles printed on FR4 substrates are presented in Figure 11.26. To obtain an antenna with a higher broadside gain and a low profile, the ground plane was replaced by a square-shaped cavity plane. Finally, the cavity was modified to a pyramid-shaped cavity and it was found out that the inclination angle should be around 45° to further improve the gain, particularly in the high-frequency band. Figure 11.27a–c illustrates the high-gain reconfigurable antenna and a comparison of three different ground planes.

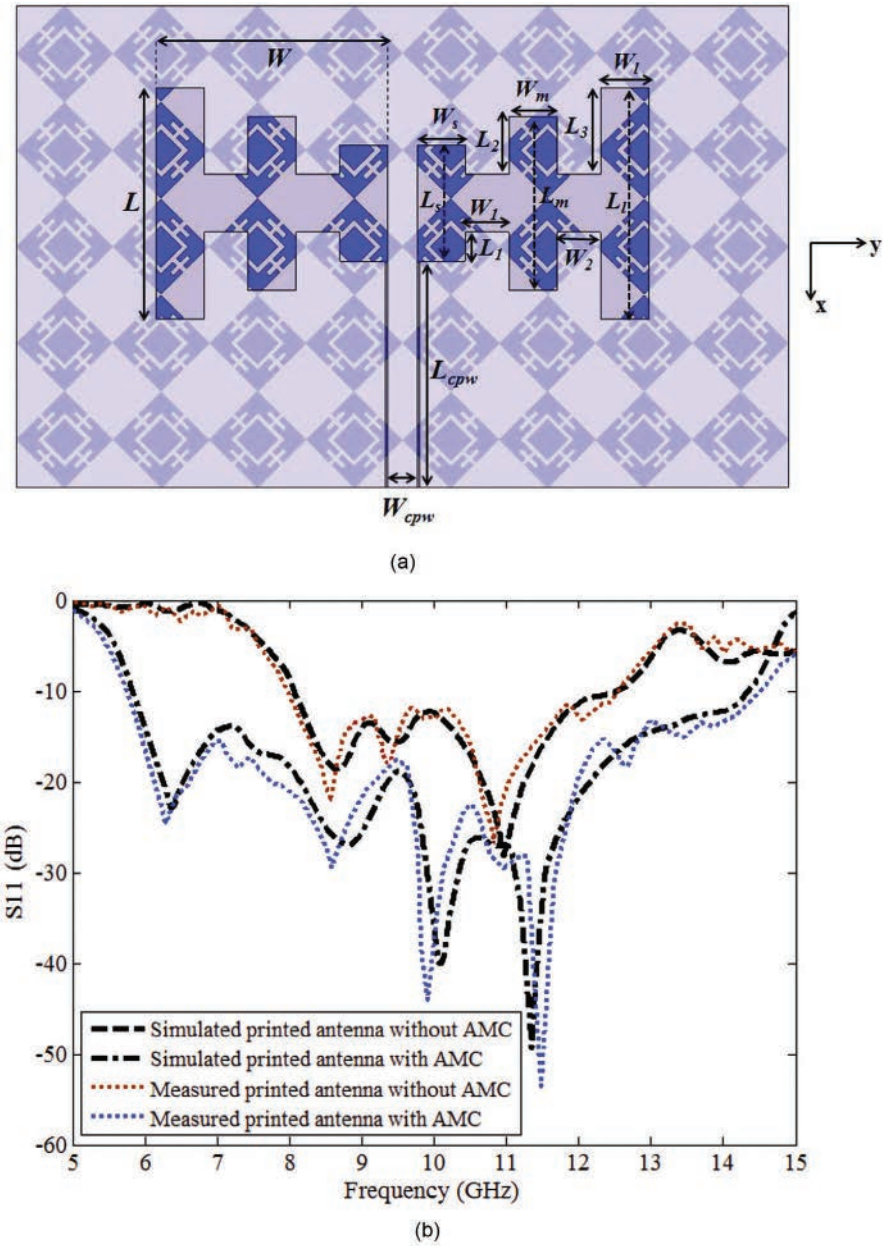

FIGURE 11.25 (a) Slot antenna with an AMC array; (b) return loss of slot antenna with an AMC array [110].

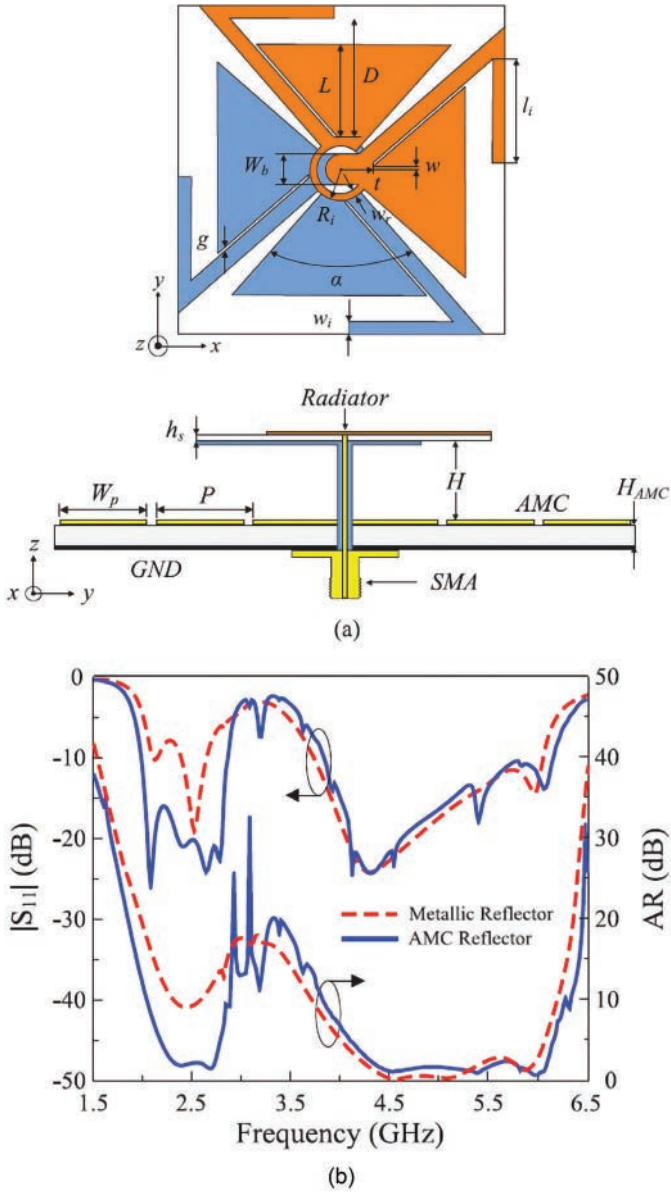

FIGURE 11.26 (a) Dual-wideband circularly polarized antenna; (b) return loss of dual-wideband circularly polarized antenna with an AMC and metallic reflector [93].

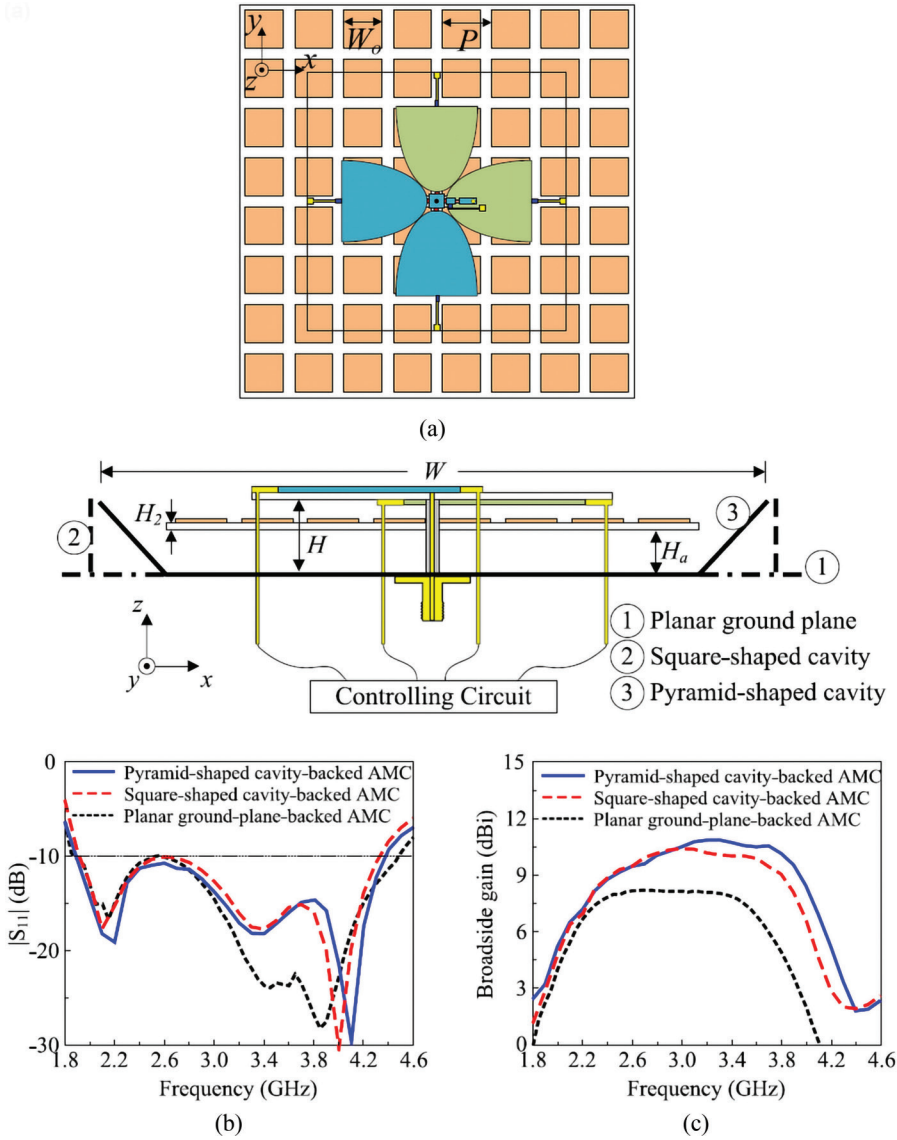

FIGURE 11.27 (a) High-gain reconfigurable antenna; (b) return loss; (c) broadside gain [96].

11.4 REAL-LIFE APPLICATIONS OF EBG PATCH ANTENNAS

11.4.1 High-Precision GPS

High-precision positioning can be achieved by combining global navigation satellite systems (GNSS) such as GPS and Galileo [97–99]. By using this system, surveyors can make measurements with sub-centimeter accuracy. In order to acquire such accurateness, some precautions are required to shield the antenna from false signals. The conventional approaches such as choke rings provide a good performance [100]. But, choke rings are generally very huge and expensive. Nowadays, EBG structures are used while maintaining good antenna performance.

A Galileo antenna on an EBG substrate is illustrated in Figure 11.28a. To achieve best gain for GPS applications, the dimension of the EBG structures is optimized. It is observed that with the combination of EBG substrate and patch antenna, an axial ratio of 2 dB is achieved. The axial ratio value for choke rings is 1 dB, which implies that the EBG patch has a better performance. Similarly, the patch and Koch fractal EBG structure [98] are shown Figure 11.28b. The tested results show the significant improvement in axial ratio bandwidth, which fits the requirement of GPS applications (Figure 11.29).

11.4.2 Wearable Electronics

Wearable electronic systems are technology that finds applications in many fields that include military, telemedicine, sports, and tracking. In [101], the jean fabric was used as a substrate having a dielectric constant of 1.7 with a thickness of 1 mm. As shown in Figure 11.29, the design consisted of a fractal monopole patch antenna with an EBG surface. This fractal antenna resonates at 1,800 MHz and 2.45 GHz for GSM and ISM applications, respectively. The antenna is placed over a 3×3 EBG array of size 150×150 mm^2. Figure 11.27 illustrates the fractal-based monopole patch antenna with an EBG surface. Another researcher used a Pellon fabric substrate [102] with a dielectric constant of 1. The designed antenna consisted of a coplanar waveguide (CPW)-fed monopole antenna with an AMC array of 4×6 units, with the overall size of 102×68 mm^2.

TABLE 11.6
Low-Profile Patch Antennas by Using Different EBG Structures

S. No.	Type of EBG Structure	Dimension (cm^3)	Height (mm)	Resonating Frequency Band	Reference
1.	EBG-CS	1.65	3	Two bands (3.5 and 4.5)	[86]
2.	Miniaturized EBG structure	4.2	0.7	One band (2.4)	[88]
3.	Square Sierpinski fractal EBG structure	10.24	1.6	Three narrow bands at 2.4, 3.5, and 4.6 GHz	[87]
4.	Uniplanar EBG structure	46.4	8	One band (1.25–29)	[95]
5.	Modified EBG structure	94.8	7.9	Two bands (2–3 and 3.8–6.3)	[93]

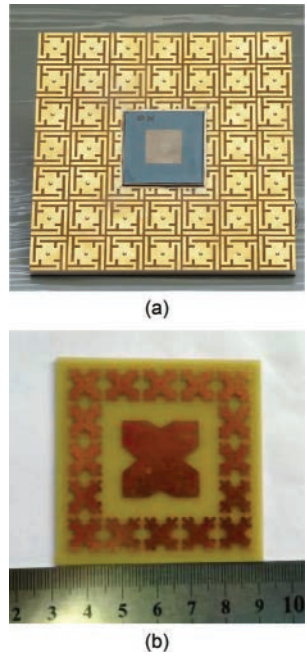

FIGURE 11.28 (a) Galileo antenna on an EBG ground plane [100]; (b) circularly polarized patch antenna with fractal HIS [102].

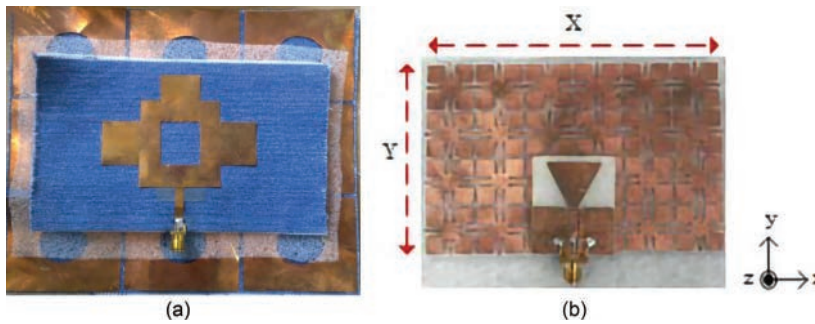

FIGURE 11.29 (a) Dual-band wearable fractal-based monopole patch antenna [101]; (b) the fabricated monopole antenna with an artificial magnetic conductor as a ground plane [102].

11.4.3 Radio Frequency Identification (RFID) Systems

RFID systems have been used since World War II, and the demand for RFID systems is rapidly growing in both business and daily life. Currently, the RFID system is used in many applications such as hospitals and healthcare, passports, stores, and people identification. One of the biggest challenges associated with RFID systems is the long-range operation capability [103–106]. In [107], a CPW-fed bow tie antenna was mounted over an AMC. The AMCs reduce the backward radiation that results in

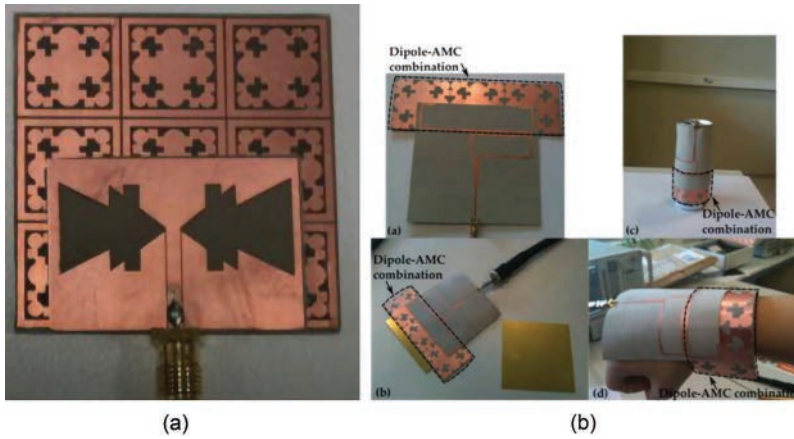

FIGURE 11.30 (a) CPW-fed bow tie antenna mounted over an AMC [107]; (b) dipole AMC [108].

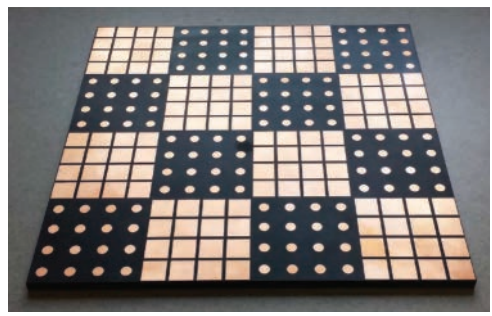

FIGURE 11.31 EBG checkerboard ground plane [109].

improved gain and directivity of the overall system. The antenna was fabricated using an ARLON 25 N substrate with a thickness of 0.7 mm and a relative permittivity of 3.3. Figure 11.30a illustrates the bow tie antenna over an AMC. This structure helps in the enhancement of gain by 2.53 and 1.86 dB at 5.8 and 6.4 GHz, respectively. In [108], a dipole antenna over an AMC was designed to improve the overall performance. From the tested results, it was observed that the dipole with a balun AMC achieved an improvement of 2.9 dBi as compared to the dipole without balun AMC.

11.4.4 Radar Systems

To reduce the radar cross section, the reflection phase property of the EBG structures is used to change the direction of the fields that are scattered by a radar target. This change in direction of the scattered fields is achieved by using checkerboard EBG structures and results in a wider frequency band RCS reduction. Figure 11.31 shows the checkerboard EBG surface which is a combination of two EBG structures.

11.5 CONCLUSION

The EBG structures have greatly attracted researchers because of their unique and desirable properties. This chapter stated how the integration of EBG structures and patch antennas improves the overall performance of the antenna systems. The recent advancements of patch antenna design using EBG structures were included. Different EBG approaches to improve gain and bandwidth were discussed. The band gap property of EBG structures has been found useful to eliminate the surface wave propagation to reduce the mutual coupling and to achieve band-notch characteristics. Real-life applications of EBG structures, such as RFID, wearable electronics, and radar systems, were also included. A number of recent publications proved that the EBG technology eliminates the drawbacks of patch antenna and is most preferable for the modern-day wireless communication systems.

REFERENCES

1. Prakash, P., Abegaonkar, M. P., Kurra, L. et al. 2015. Compact electromagnetic band-gap (EBG) structure with defected ground. *IETE Journal of Research*. 62:120–126.
2. Yang, F.-R. 1999. A uniplanar compact photonic-bandgap (UC-PBG) structure and its applications for microwave circuits. *IEEE Transactions on Microwave Theory and Techniques*. 47:1–6.
3. Yang, F. and Samii, Y. R. 2003. Microstrip antennas integrated with electromagnetic band-gap (EBG) structures: A low mutual coupling design for array applications. *IEEE Transactions on Antennas and Propagation*. 51:2936–2946.
4. Shaban, H. F., Elmikaty, H. A. and Shaalan, A. A. 2008. Study the effects of electromagnetic band-gap (EBG) substrate on two patches microstrip antenna. *Progress in Electromagnetics Research B*. 10:1–20.
5. Alshamaileh, K. A., Almalkawi, M. J. and Devabhaktuni, V. K. 2015. Dual band-notched microstrip-fed vivaldi antenna utilizing compact EBG structures. *International Journal of Antennas and Propagation*. 2015:1–7.
6. Loinaz, A. I. and Bocio, C. R. 2004. EBG at microwave frequency range: Bragg and/or resonant effect. *Microwave and Optical Technology Letters*. 42:383–385.
7. Jaglan, N. and Gupta, S. D. 2015. Reflection phase characteristics of EBG structures and WLAN band notched circular monopole antenna design. *International Journal on Communications Antenna and Propagation (IRECAP)*. 5:201–233.
8. Kumar, A., Kumar, D., Mohan, J. et al. 2015. Investigation of grid metamaterial and EBG structures and its application to patch antenna. *International Journal of Microwave and Wireless Technologies*. 7:705–712.
9. Kaabal, A. M., Halaoui, E., Ahyoud, S. et al. 2016. Dual band-notched WIMAX/WLAN of a compact UltraWide Band antenna with spectral and time domains analysis for breast cancer detection. *Progress in Electromagnetics Research C*. 65:163–173.
10. Palreddy, S. 2015. Wideband electromagnetic band gap (EBG) structures, analysis and applications to antennas. Virginia Polytechnic Institute 4:1–131.
11. Choi, J. H., Hon, P. W. C. and Itoh, T. 2014. Dispersion analysis and design of planar electromagnetic bandgap ground plane for broadband common-mode suppression. *IEEE Microwave and Wireless Components Letters*. 24:772–774.
12. Bhavarthe, P. P., Rathod, S. S. and Reddy, K. T. V. 2017. A compact two via slot-type electromagnetic bandgap structure. *IEEE Microwave and Wireless Components Letters*. 27:446–448.

13. Huang, C., Ji, C., Wu, X. et al. 2018. Combining FSS and EBG surfaces for high-efficiency transmission and low-scattering properties. *IEEE Transactions on Antennas and Propagation*. 66:1628–1632.
14. Alam, M. S., Misran, N. and Yatim, B. 2013. Development of electromagnetic band gap structures in the perspective of microstrip antenna design. *International Journal of Antennas and Propagation*. 1–22. Article ID 507158.
15. Zhou, Z., Wei, Z., Tang, Z., and Yin Y. 2019. Design and analysis of a wideband multiple microstrip dipole antenna with high isolation. *IEEE Antennas and Wireless Propagation Letters*. 18: 722–726.
16. Guo, Z., Tian, H., Wang, X. et al. 2013. Bandwidth enhancement of monopole UWB antenna with new slots and EBG structures. *IEEE Antennas and Wireless Propagation Letters*. 12:1550–1553.
17. Baudha, S. and Vishwakarma, D. K. 2016. Bandwidth enhancement of a planar monopole microstrip patch antenna. *International Journal of Microwave and Wireless Technologies*. 8:237–242.
18. Alkhatib, R. and Drissi, M. 2007. Improvement of bandwidth and efficiency for directive superstrate EBG antenna. *Electronics Letters*. 43:694–702.
19. Denidni, T. A. Coulibaly, Y. and Boutayeb, H. 2009. Hybrid dielectric resonator antenna with circular mushroom-like structure for gain improvement. *IEEE Transactions on Antennas and Propagation*. 57:1043–1049.
20. Alrabadi, O., Perruisseau-Carrier, N. J. and Kalis, A. 2012. MIMO transmission using a single RF source: Theory and antenna design. *IEEE Transactions on Antennas and Propagation*. 60:654–664.
21. Braaten, B. D., Iftikhar, A., Capobianco, A. D. et al. 2015. Compact 4×4 UWB-MIMO antenna with WLAN band rejected operation. *Electronics Letters*. 51:1048–1050.
22. Kiem, N. K., Phuong, H. N. B. and Chien, D. N. 2014. Design of compact 4×4 UWB-MIMO antenna with WLAN band rejection. *International Journal of Antennas and Propagation*. 1–11. Article ID 539094.
23. Zhang, S. and Pedersen, G. F. 2016. Mutual coupling reduction for UWB MIMO antennas with a wideband neutralization line. *IEEE Antennas and Wireless Propagation Letters*. 15:166–169.
24. Elsheakh, D. N., Elsadek, H. A., Abdallah, E. et al. 2009. Enhancement of microstrip monopole antenna bandwidth by using EBG structures. *IEEE Antennas and Wireless Propagation Letters*. 8:959–962.
25. Gujral, M. J., Li, L.-W., Yuan, W. et al. 2012. Bandwidth improvement of microstrip antenna array using dummy EBG pattern on feedline. *Progress in Electromagnetics Research*. 127:79–92.
26. Wen, B.-J., Peng, L., Li, X.-F. et al. 2019. A low-profile and wideband unidirectional antenna using bandwidth enhanced resonance-based reflector for fifth generation (5G) systems applications. *IEEE Access*. 7:27352–27361.
27. Madhav, B. T. P., Sanikommu, M. M., Pranoop, N. V. et al. 2015. CPW fed antenna for wideband applications based on tapered step ground and EBG structure. *Indian Journal of Science and Technology*. 8:101–119.
28. Kim, M. 2015. A compact EBG structure with wideband power/ground noise suppression using meander-perforated plane. *IEEE Transactions on Electromagnetic Compatibility*. 57:595–598.
29. Shen, C.-K., Chen, C.-H., Han, D.-H. et al. 2015. Modeling and analysis of bandwidth-enhanced multilayer 1-D EBG with bandgap aggregation for power noise suppression. *IEEE Transactions on Electromagnetic Compatibility*. 57:858–867.
30. Yang, Q., Wang, X., Wang, J. J. et al. 2011. Reducing SAR and enhancing cerebral signal-to-noise ratio with high permittivity padding at 3 T. *Magnetic Resonance in Medicine*. 65:358–362.

31. Wang, C.-D. 2012. Bandwidth enhancement based on optimized via location for multiple vias EBG power/ground planes. *IEEE Transactions on Components, Packaging and Manufacturing Technology*. 2:332–341.
32. Taha, E. A., Ahmed, I. I. and Yahiea, A. 2015. A miniaturized lotus shaped microstrip antenna loaded with EBG structures for high gain-bandwidth product applications. *Progress in Electromagnetics Research C*. 60:157–167.
33. Cos, M. E. and Heras, F. L. 2012. Dual-band uniplanar CPW-fed monopole/EBG combination with bandwidth enhancement. *IEEE Antennas and Wireless Propagation Letters*. 11:365–368.
34. Jam, S. and Simruni, M. 2018. Performance enhancement of a compact wideband patch antenna array using EBG structures. *AEU – International Journal of Electronics and Communications*. 89:42–55.
35. Shoaib, N., Shoaib, S. R., Khattak, Y. et al. 2018. MIMO antennas for smart 5G devices. *IEEE Access*. 67:7014–77021.
36. Peddakrishna, S., Khan, T. and De, A. 2017. Electromagnetic band-gap structured printed antennas: A feature oriented survey. *International Journal RF Microwave Computational Aided Engineering*. 27:1–16.
37. Hadarig, R. C., de Cos, M. E. and Las-Heras, F. 2013. Novel miniaturized artificial magnetic conductor. *IEEE Antennas and Wireless Propagation Letters*. 12:174–177.
38. Khan, M. S., Tahir, F. A., Meredov, A. et al. 2019. A W-band EBG-backed double-rhomboid bowtie-slot on-chip antenna. *IEEE Antennas and Wireless Propagation Letters*. 18:1046–1050.
39. McKinzie, W. E., Nair, D. M., Thrasher, B. A. et al. 2016. 60-GHz LTCC patch antenna array with an integrated EBG structure for gain enhancement. *IEEE Antennas and Wireless Propagation Letters*. 15:1522–1525.
40. Chen, D., Yang, W. and Che, W. 2018. High-gain patch antenna based on cylindrically projected EBG planes. *IEEE Antennas and Wireless Propagation Letters*. 17:2374–2378.
41. Bhavarthe, P. P., Rathod, S. S. and Reddy, K. T. V. 2018. A compact two-via hammer spanner-type polarization-dependent electromagnetic bandgap structure. *IEEE Microwave and Wireless Components Letters*. 28:284–286.
42. Ketkuntod, P., Hongnara, T. Thaiwirot, W. et al. 2017. Gain enhancement of microstrip patch antenna using I-shaped mushroom-like EBG structure for WLAN application. In *2017 International Symposium on Antennas and Propagation (ISAP)*. 1–2.
43. Bharathi, M. and Phavithra, P. J. 2018. Gain enhancement of a square patch antenna using EBG structure. *International Journal of Innovative Technology and Exploring Engineering*. 8:1–4.
44. Boutayeb, H. and Denidni, T. A. 2007. Gain enhancement of a microstrip patch antenna using a cylindrical electromagnetic crystal substrate. *IEEE Transactions on Antennas and Propagation*. 55:3140–3145.
45. Mondal, K. and Sarkar, P. P. 2019. Gain and bandwidth enhancement of microstrip patch antenna for WiMAX and WLAN applications. *IETE Journal of Research*. 1–9.
46. Mark, R., Rajak, N. Mandal, K. et al. 2019. Metamaterial based superstrate towards the isolation and gain enhancement of MIMO antenna for WLAN application. *AEU – International Journal of Electronics and Communications*. 100:144–152.
47. Han, Z.-J., Song, W. and Sheng, X.-Q. 2017. Gain enhancement and RCS reduction for patch antenna by using polarization-dependent EBG surface. *IEEE Antennas and Wireless Propagation Letters*. 16:1631–1634.
48. Liu, Z., Liu, Y. and Gong, S. 2018. Gain enhanced circularly polarized antenna with RCS reduction based on metasurface. *IEEE Access*. 6:46856–46862.

49. Roseline, A., Malathi, K. and Shrivastav, A. K. 2011. Enhanced performance of a patch antenna using spiral-shaped electromagnetic bandgap structures for high-speed wireless networks. *IET Microwaves, Antennas & Propagation*. 5:1733–1750.
50. Lee, Y. J., Yeo, J., Mittra, R. et al. 2005. Application of electromagnetic bandgap (EBG) superstrates with controllable defects for a class of patch antennas as spatial angular filters. *IEEE Transactions on Antennas and Propagation*. 53: 224–235.
51. Haraz, O., Elboushi, M., Alshebeili, A. et al. 2014. Dense dielectric patch array antenna with improved radiation characteristics using EBG ground structure and dielectric superstrate for future 5G cellular networks. *IEEE Access*. 2:909–913.
52. Yang, X., Liu, Y., Xu, Y.-X. et al. 2017. Isolation enhancement in patch antenna array with fractal UC-EBG structure and cross slot. *IEEE Antennas and Wireless Propagation Letters*. 16:2175–2178.
53. Mohamed, I., Abdalla, M. and Mitkees, A. E. 2019. Perfect isolation performance among two-element MIMO antennas. *AEU – International Journal of Electronics and Communications*. 107:21–31.
54. Mohamadzade, B. and Afsahi, M. 2017. Mutual coupling reduction and gain enhancement in patch array antenna using a planar compact electromagnetic bandgap structure. *IET Microwaves, Antennas & Propagation*. 11:1719–1725.
55. Li, Q., Feresidis, A. P., Mavridou, M. et al. 2015. Miniaturized double-layer EBG structures for broadband mutual coupling reduction between UWB monopoles. *IEEE Transactions on Antennas and Propagation*. 63:1168–1171.
56. Tan, X., Wang, W., Wu, Y. Y. et al. 2019. Enhancing isolation in dual-band meander-line multiple antenna by employing split EBG structure. *IEEE Transactions on Antennas and Propagation*. 67:2769–2774.
57. Arshed, T. and Tahir, F. A. 2017. A miniaturized triple band-notched UWB antenna. *Microwave and Optical Technology Letters*. 59:2581–2586.
58. Toyota, Y. A., Engin, E. T., Kim, H. et al. 2006. Stopband analysis using dispersion diagram for two-dimensional electromagnetic bandgap structures in printed circuit boards. *IEEE Microwave and Wireless Components Letters*. 16:645–647.
59. Farahani, H., Veysi, S., Kamyab, M. et al. 2010. Mutual Coupling reduction in patch antenna arrays using a UC-EBG superstrate. *IEEE Antennas and Wireless Propagation Letters*. 9:57–59.
60. Alibakhshikenari, M., Khalily, M. B., Virdee, B. S. et al. 2019. Mutual coupling suppression between two closely placed microstrip patches using EM-bandgap metamaterial fractal loading. *IEEE Access*. 7:23606–23614.
61. Kumar, N. and Kommuri, U. K. 2019. MIMO antenna H-plane isolation enhancement using UC-EBG structure and metal line strip for WLAN applications. *Radioengineering*. 27:399–406.
62. Mavridou, M., Feresidis, A. P. and Gardner, P. 2016. Tunable double-layer EBG structures and application to antenna isolation. *IEEE Transactions on Antennas and Propagation*. 64:70–79.
63. Kushwaha, N. and Kumar, R. 2013. An UWB fractal antenna with defected ground structure and swastika shape electromagnetic band gap. *Progress in Electromagnetics Research B*. 52:383–403.
64. Jaglan, N., Kanaujia, B. K., Gupta, S. D. et al. 2016. Triple band notched UWB antenna design using electromagnetic band gap structures. *Progress in Electromagnetics Research C*. 66:139–147.
65. Pandey, G. K., Singh, H. S., Bharti, P. K. et al. 2013. Design of WLAN band notched UWB monopole antenna with stepped geometry using modified EBG structure. *Progress in Electromagnetics Research B*. 50:201–217.

66. Mouhouche, F., Azrar, A., Dehmas, M. et al. 2018. Design a compact UWB monopole antenna with triple band-notched characteristics using EBG structures. *Frequenz*. 11:479–487.
67. Peng, L. and Ruan, C.-L. 2011. UWB band-notched monopole antenna design using electromagnetic-bandgap structures. *IEEE Transactions on Microwave Theory and Techniques*. 59:1074–1081.
68. Mandal, T. and Das, S. 2014. Design of dual notch band UWB printed monopole antenna using electromagnetic-bandgap structure. *Microwave and Optical Technology Letters*. 56:2195–2199.
69. Jaglan, N., Gupta, S. D., Thakur, E. et al. 2018. Triple band notched mushroom and uniplanar EBG structures based UWB MIMO/Diversity antenna with enhanced wide band isolation. *AEU – International Journal of Electronics and Communications*. 90:36–44.
70. Jaglan, N., Kanaujia, B. K., Gupta, S. D. et al. 2017. Dual band notched EBG structure based UWB MIMO/diversity antenna with reduced wide band electromagnetic coupling. *Frequenz*. 71:11–12.
71. Liu, H. and Xu, Z. 2013. Design of UWB monopole antenna with dual notched bands using one modified electromagnetic-bandgap structure. *The Scientific World Journal*. 2013:1–9.
72. Wang, J. H., Yin, Y.-Z. and Liu, X. L. 2013. Triple band-notched ultra wideband (UWB) antenna using a novel modified capacitively loaded loop (CLL) resonator. *Progress in Electromagnetics Research Letters*. 42:55–64.
73. Li, T., Zhai, H.-Q., Li, G.-H. et al. 2012. Design of compact UWB band-notched antenna by means of electromagnetic-bandgap structures. *Electronics Letters*. 48:601–608.
74. Ghosh, A., Mandal, T. and Das, S. 2019. Design and analysis of triple notch ultrawideband antenna using single slotted electromagnetic bandgap inspired structure. *Journal of Electromagnetic Waves and Applications*. 33:1391–1405.
75. Jaglan, N., Gupta, S. D., Kanaujia, B. K. et al. 2018. Band notched UWB circular monopole antenna with inductance enhanced modified mushroom EBG structures. *Wireless Networks*. 24:383–393.
76. Jaglan, N., Kanaujia, B. K., Gupta, S. D. et al. 2018. Design of band-notched antenna with DG-CEBG. *International Journal of Electronics*. 105:58–72.
77. Peddakrishna, S. and Khan, T. 2018. Design of UWB monopole antenna with dual notched band characteristics by using π-shaped slot and EBG resonator. *AEU – International Journal of Electronics and Communications*. 96:107–112.
78. Zhang, X. 2018. Design of defective electromagnetic band-gap structures for use in dual-band patch antennas. *International Journal of RF and Microwave Computer-Aided Engineering*. 28:22126–21287.
79. Yi, H. and Qu, S.-W. 2013. A novel dual-band circularly polarized antenna based on electromagnetic band-gap structure. *IEEE Antennas and Wireless Propagation Letters*. 12:1149–1152.
80. Saurav, K., Sarkar, D. and Srivastava, K. V. 2014. Dual-polarized dual-band patch antenna loaded with modified mushroom unit cell. *IEEE Antennas and Wireless Propagation Letters*. 13:1357–1360.
81. Emadian, S. R. and Shokouh, J. A. 2015. Very small dual band-notched rectangular slot antenna with enhanced impedance bandwidth. *IEEE Transactions on Antennas and Propagation*. 63:4529–4534.
82. Liu, T. H., Zhang, W. X., Zhang, M. et al. 2000. Low profile spiral antenna with PBG substrate. *Electronics Letters*. 36:773–779.
83. Yousefi, L., Mohajer-Iravani, B. and Ramahi, O. M. 2007. Low profile wide band antennas using electromagnetic bandgap structures with magneto-dielectric materials. *International workshop on Antenna Technology: Small and Smart Antennas Metamaterials and Applications*. 431–434.

84. Li, L., Li, B., Liu, H.-X. et al. 2006. Locally resonant cavity cell model for electromagnetic band gap structures. *IEEE Transactions on Antennas and Propagation*. 54:90–100.
85. Ghabzouri, M., El Salhi, A. E., Anacleto, P. et al. 2017. Enhanced low profile, dual-band antenna via novel electromagnetic band gap structure. *Progress in Electromagnetics Research C*. 71:79–89.
86. Ma, X., Mi, S. and Lee, Y. H. 2015. Design of a microstrip antenna using square Sierpinski fractal EBG structure. *IEEE 4th Asia-Pacific Conference on Antenna and Propagation (APCAP)*.
87. Ashyap, A. Y. I. 2017. Compact and low-profile textile EBG-based antenna for wearable medical applications. *IEEE Antennas and Wireless Propagation Letters*. 16:2550–2553.
88. Li, Z. and Samii, Y. R. 2000. PBG, PMC and PEC ground planes: a case study of dipole antennas. *IEEE Antennas and Propagation Society International Symposium. Transmitting Waves of Progress to the Next Millennium. 2000 Digest. Held in conjunction with: USNC/URSI National Radio Science Meeting (Cat. No.00CH37118)*. 2: 674–677.
89. Cao, W., Zhang, B., Liu, A. et al. 2012. Multi-frequency and dual-mode patch antenna based on electromagnetic band-gap (EBG) structure. *IEEE Transactions on Antennas and Propagation*. 60:6007–6012.
90. Kasahara, Y., Toyao, H. and Hankui, E. 2017. Compact and multiband electromagnetic bandgap structures with adjustable bandgaps derived from branched open-circuit lines. *IEEE Transactions on Microwave Theory and Techniques*. 65:2330–2340.
91. Misran, N., Islam, M. T. and Alam, M. S. 2013. Inverse triangular-shape CPW-fed antenna loaded with EBG reflector. *Electronics Letters*. 49:86–88.
92. Tran, H. H. and Park, I. 2016. A dual-wideband circularly polarized antenna using an artificial magnetic conductor. *IEEE Antennas and Wireless Propagation Letters*. 15:950–953.
93. Chamani, Z. and Jahanbakht, S. 2017. Improved performance of double-t monopole antenna for 2.4/5.6 GHz dual-band WLAN operation using artificial magnetic conductors. *Progress in Electromagnetics Research M*. 61:205–213.
94. Lin, W., Chen, S.-L., Ziolkowski, R. W. et al. 2018. Reconfigurable, wideband, low-profile, circularly polarized antenna and array enabled by an artificial magnetic conductor ground. *IEEE Transactions on Antennas and Propagation*. 66:1564–1569.
95. Tran, H. H., Trong, N. N., Le, T. T. et al. 2018. Low-profile wideband high-gain reconfigurable antenna with quad-polarization diversity. *IEEE Transactions on Antennas and Propagation*. 66:3741–3746.
96. Bao, X. L., Ruvio, G. and Ammann, M. J. 2007. Low-profile dual-frequency GPS patch antenna enhanced with dual-band EBG structure. *Microwave and Optical Technology Letters*. 49:2630–2634.
97. Wang, E. and Liu, Q. 2016. GPS patch antenna loaded with fractal EBG structure using organic magnetic substrate. *Progress in Electromagnetics Research Letters*. 58:23–28.
98. Srivastava, R. 2014. Dual band rectangular and circular slot loaded microstrip antenna for WLAN/GPS/WiMax applications. *2014 Fourth International Conference on Communication Systems and Network Technologies*. 45–48.
99. Baggen, R. M., Vazquez, M. J., Leiss, J. et al. 2008. Low profile GALILEO antenna using EBG technology. *IEEE Transactions on Antennas and Propagation*. 56:667–674.
100. Velan, S. 2015. Dual-band EBG integrated monopole antenna deploying fractal geometry for wearable applications. *IEEE Antennas and Wireless Propagation Letters*. 14:249–252.
101. Alemaryeen, A. and Noghanian, S. 2019. On-body low-profile textile antenna with artificial magnetic conductor. *IEEE Transactions on Antennas and Propagation*. 67:3649–3656.

102. Phatarachaisakul, T., Pumpoung, T. and Phongcharoenpanich, C. 2005. Dual-band RFID tag antenna with EBG for glass objects. *IEEE 4th Asia-Pacific Conference on Antennas and Propagation (APCAP)*. 199–200.
103. Ukkonen, L., Sydanheimo, L. and Kivikoski, M. 2004. Patch antenna with EBG ground plane and two-layer substrate for passive RFID of metallic objects. *IEEE Antennas and Propagation Society Symposium*. 1:93–96.
104. Phatra, C., Krachodnok, P. and Wongsan, R. 2009. Design of a RFID tag using dipole antenna with Electromagnetic Band Gap. *International Conference on Electrical Engineering/Electronics, Computer, Telecommunications and Information Technology*. 1:1–4.
105. Konishi, T., Miura, T., Numata, Y. et al. 2009. An impedance matching technique of a UHF-band RFID tag on a high-impedance surface with parasite elements. *IEEE Radio and Wireless Symposium*. 67–70.
106. Cos, M. E. and Las-Heras, F. 2012. Dual-band antenna/AMC combination for RFID. *International Journal of Antennas and Propagation*. 2012:1–7.
107. Hadarig, R. C., de Cos, M. E. and Las-Heras, F. 2013. UHF dipole-AMC combination for RFID applications. *IEEE Antennas and Wireless Propagation Letters*. 12:1041–1044.
108. Simruni, M. and Jam, S. 2019. Radiation performance improvement of wideband microstrip antenna array using wideband AMC structure. *International Journal of Communication Systems*. 32:3954–3962.
109. Hossein, M. and Shahrokh, J. 2016. Improved radiation performance of low profile printed slot antenna using wideband planar AMC surface. *IEEE Transactions on Antennas and Propagation*. 64:4626–4638.